



1 **Nano-hygroscopicity tandem differential mobility analyzer (nano-HTDMA) for**
2 **investigating hygroscopic properties of sub-10 nm aerosol nanoparticles**

3 Ting Lei^{1,2}, Nan Ma^{4,1,3}, Juan Hong^{4,1}, Thomas Tuch³, Xin Wang², Zhibin Wang⁵, Mira Pöhlker², Maofa
4 Ge⁶, Weigang Wang⁶, Eugene Mikhailov⁷, Thorsten Hoffmann⁸, Ulrich Pöschl², Hang Su², Alfred
5 Wiedensohler³, Yafang Cheng¹

6 ¹Minerva Research Group, Max Planck Institute for Chemistry, 55128 Mainz, Germany

7 ²Multiphase Chemistry Department, Max Planck Institute for Chemistry, 55128 Mainz, Germany

8 ³Leibniz Institute for Tropospheric Research, 04318 Leipzig, Germany

9 ⁴Institute for Environmental and Climate Research, Jinan University, 511443 Guangzhou, China

10 ⁵Reserch Center for Air Pollution and Health, College of Environmental and Resource Science, Zhejiang University, Hangzhou,
11 310058, China

12 ⁶Beijing National Laboratory for Molecular Sciences (BNLMS), Institute of Chemistry, Chinese Academy of Sciences, Beijing,
13 100190, P. R. China

14 ⁷St. Petersburg State University, 7/9 Universitetskaya nab., St. Petersburg, 199034, Russia

15 ⁸Institute of Inorganic Chemistry and Analytical Chemistry, Johannes Gutenberg University Mainz, Mainz, Germany

16

17 *Correspondence to:* Yafang Cheng (yafang.cheng@mpic.de) and Juan Hong (juanhong0108@jnu.edu.cn)

18

19 **Abstract.** Interactions between water and nanoparticles are relevant for atmospheric multiphase processes,
20 physical chemistry, and materials science. Current knowledge of the hygroscopic and related physico-
21 chemical properties of nanoparticles, however, is restricted by limitations of the available measurement
22 techniques. Here, we present the design and performance of a nano-hygroscopicity tandem differential
23 mobility analyzer (nano-HTDMA) apparatus that enables high accuracy and precision in hygroscopic
24 growth measurements of aerosol nanoparticles with diameters less than 10 nm. Detailed methods of
25 calibration and validation are provided. Beside maintaining accurate and stable sheath/aerosol flow rates
26 ($\pm 1\%$), high accuracy of DMA voltage ($\pm 0.1\%$) in the range of ~ 0 -50 V is crucial to achieve accurate sizing
27 and small sizing offsets between the two DMAs ($< 1.4\%$). To maintain a stable relative humidity (RH), the



28 humidification system and the second DMA are placed in a well-insulated and air conditioner housing
29 ($\pm 0.1K$). We also tested and discussed different ways of preventing pre-deliqescence in the second DMA.
30 Our measurement results for ammonium sulfate nanoparticles are in good agreement with Biskos et al.
31 (2006b), with no significant size-effect on the deliquescence and efflorescence relative humidity (DRH,
32 ERH) at diameters down to 6 nm. For sodium sulfate nanoparticles, however, we find a pronounced size-
33 dependence of DRH and ERH between 20 and 6 nm nanoparticles.

34

35 **1 Introduction**

36 The climatic effects of aerosol nanoparticles have attracted increasing interests in recent years (Wang et
37 al., 2016; Andreae et al., 2018; Fan et al., 2018). Aerosol nanoparticles in the atmosphere are mostly
38 originating from new particle formation, and a fraction of these nanoparticles could potentially grow into
39 sizes to efficiently act as cloud condensation nuclei and thus to change the contributions of aerosol
40 nanoparticles to climate forcing (Lihavainen 2003; Wiedensohler et al., 2009; Sihto et al., 2011; Kirkby et
41 al., 2011; Keskinen et al., 2013; Dunne et al., 2016; Kim et al., 2016). These processes strongly depend on
42 the chemical composition and physico-chemical properties of these nanoparticles (Köhler, 1936; Su et al.,
43 2010; Wang et al., 2015; Cheng et al., 2015). One of the most important physico-chemical properties of
44 nanoparticles is their hygroscopic behavior that describes their ability to take up water, and it can differ
45 significantly from that of larger particles (Hämeri et al., 2000, 2001; Gao et al., 2006; Biskos et al., 2006a,
46 b, 2007; Cheng et al., 2015).

47 To understand and predict hygroscopic properties of nanoparticles, current thermodynamic models mostly
48 rely on the concentration-dependent thermodynamic properties (such as water activity and interfacial
49 energy) derived from the measurements of large aerosol particles or even bulk samples (Tang and
50 Munkelwitz, 1994; Tang 1996; Pruppacher and Klett, 1997; Clegg et al., 1998). They are thus difficult or
51 impossible to be applied to describe the hygroscopic behavior of sub-10 nm particles which can be often



52 supersaturated in concentration compared to bulk solutions (Cheng et al., 2015). Furthermore, the nanosize
53 effect on these properties may also need to be considered (Cheng et al., 2015). The lack of such data hinders
54 the understanding and an accurate simulation of the interaction of water vapor and atmospheric
55 nanoparticles. In addition, by knowing the hygroscopicity of newly formed nanoparticle, one can infer the
56 involving chemical species (e.g., organic ratio) in particle formation and initial growth (Wang et al., 2010),
57 which is otherwise difficult and highly challenge to measure directly (Wang et al., 2010; Ehn et al., 2014).
58 Hence, to measure the hygroscopicity of nanoparticles is essential to improve our understandings of aerosol
59 formation, transformation, and their climate effects.

60 Different techniques have been employed to characterize the hygroscopic properties of aerosol particles in
61 different sizes (Fig. S1) (Tang et al., 2019), such as Fourier transform infrared spectrometer (FT-IR) (Zhao
62 et al., 2006), Raman spectroscopy (Dong et al., 2009), electrodynamic balance (EDB) (Chan and Chan,
63 2003, 2005; Chan et al., 2008), optical tweezers (Reid et al., 2011; Rickards et al., 2013), hygroscopicity
64 tandem differential mobility analyzer (HTDMA) (e.g., Rader and McMurry, 1986; Mikhailov et al., 2004;
65 2008; 2009; Biskos et al., 2006a, b, 2007; Cheng et al., 2008, 2009; Eichler et al., 2008; Stock et al., 2011;
66 Hong et al., 2014, 2015; Lei et al., 2014; 2018; Mikhailov and Vlasenko, 2019), and atomic force
67 microscopy (AFM) (Estillore et al., 2017). Using these techniques, most of the early lab studies focuses
68 on the hygroscopic behavior of particles in accumulation modes and super-micron size range, including
69 deliquescence, efflorescence of pure components and the effect of organics on the change or suppression
70 of deliquescence and efflorescence of these inorganic components in mixtures.

71 For nanoparticles with diameters down to sub-10 nm, there are, however, only very few studies attempting
72 to investigate their interactions with water molecules, which mainly utilized the setup with humidified
73 tandem DMAs (Hämeri et al., 2000, 2001; Sakurai et al., 2005; Biskos et al., 2006a, b, 2007; Giamarelou
74 et al., 2018). In Table S1, we summarized the measured DRH and ERH of ammonium sulfate nanoparticles
75 in the size range from 6 to 100 nm using HTDMAs. In these studies, the results of the observed



76 deliquescence and efflorescence relative humidity (respective DRH and ERH) and prompt or non-prompt
77 phase transitions of ammonium sulfate nanoparticles, however, do not show universal agreement. The
78 technical challenges in HTDMA measurements, especially in the sub-10 nm size range, mainly lie on: (1)
79 accurate sizing and small sizing offset of the two DMAs, (2) highly stable measurement conditions in the
80 whole system. Large sizing offset between the two DMAs may lead to significant error in the measured
81 growth factor based on error propagation (Mochida and Kawamura, 2004). Massling et al. (2011) and
82 Zhang et al. (2016) suggested that to achieve good hygroscopic growth factor of nanoparticles, the sizing
83 offset of the two DMAs should be within $\pm 2-3\%$, which is however very difficult to maintain for the sub-
84 10 nm size range. To accurately measure phase transition (e.g., DRH and ERH), a highly stable
85 measurement condition is essential, especially maintaining a small temperature perturbation in the
86 humidification system and inside the second DMA to prevent pre-deliqescence. For example, a 0.8 K
87 fluctuation of the experimental temperature during the measurement can result in a 4% difference in RH
88 (0-90%) inside the humidified DMA (Hämeri et al., 2000), leading to an inaccurate determination of the
89 phase transition. Another problem is the prompt versus non-prompt phase transition. Although effects of
90 impurities on the phase transition of aerosol nanoparticles (Biskos et al., 2006a; Russell and Ming, 2002)
91 may be one possible reason of the previously observed non-prompt phase transitions (e.g., Hämeri et al.,
92 2000), the apparent non-prompt phase transition of aerosol nanoparticles has been thought to be mainly due
93 to the inhomogeneity of RH and temperature in the humidified DMA during measurements (Biskos et al.,
94 2006b; Bezantakos et al., 2016). Moreover, the hygroscopic measurements are in general difficult for
95 nanoparticles with diameters below 20 nm due to high diffusion losses of nanoparticles (Seinfeld and
96 Pandis, 2006).

97 In this study, we present a design of nano-HTDMA setup that enables high accuracy and precision in
98 hygroscopic growth measurements of aerosol nanoparticles with diameters less than 10 nm. Detailed
99 methods of calibration and validation are provided. We discuss in detail how to maintain the good
100 performance of the system by minimizing uncertainties associated with the stability and accuracy of RH,



101 temperature, voltage for nanoparticle classification, and sheath and aerosol flows in the DMA systems. We
102 then apply the nano-HTDMA system to study the size dependence of the deliquescence and the
103 efflorescence of aerosol nanoparticles of two specific inorganic compounds (e.g., ammonium sulfate and
104 sodium sulfate) for sizes down to 6 nm.

105

106 **2. Methods**

107 **2.1 Nano-HTDMA system**

108 A nano-HTDMA system is built up to measure the aerosol nanoparticle hygroscopic growth factor (g_r),
109 especially aiming for accurate measurement of phase transition and hygroscopic growth factor for
110 nanoparticles in the sub-10 nm size range. Here, g_r is defined as the ratio of mobility diameters of
111 nanoparticles after humidification ($D_m(RH)$) to that at dry condition ($D_m(< 10\% RH)$) (see SI. Eq. (S1)).
112 As presented in Fig. 1, the nano-HTDMA composes three main components, including two nano-
113 differential mobility analyzers (nano-DMA, TROPOS Model Vienna-type short DMA; Birmili et al., 1997),
114 an ultrafine condensation particle counter (CPC, TSI Model 3776), and a humidification system. Table 1
115 shows the technical specification, where the DMA system, humidification system, and temperature system
116 of the three HTDMAs setup are compared among the systems of Biskos et al. (2006b), Hämeri et al. (2000)
117 and this study.

118 In our setup (Fig. 1), the first nano-DMA (nano-DMA1) is used to produce quasi-monodisperse
119 nanoparticles at a desired dry diameter. The flow rate of the closed-loop sheath flow in the nano-DMA1 is
120 maintained at 10 l/min. The ratio of sheath flow to aerosol flow is 10:1.5. The sheath flow is dried to RH
121 below 10% by two custom-built Nafion dryers (TROPOS Model ND.070) in parallel. The quasi-
122 monodisperse nanoparticles produced by nano-DMA1 then enter the humidification system, which can be
123 set to deliquescence mode (from low RH to high RH for measuring deliquescence) or efflorescence mode



124 (from high RH to low RH for measuring efflorescence). In the deliquescence mode, dry nanoparticles are
125 humidified by a Nafion humidifier (NH-1, TROPOS Model ND.070, L. 24") to a target RH. In the
126 efflorescence mode, nanoparticles are first exposed to a high RH condition (~97% RH) in a Nafion
127 humidifier (NH-2, Perma Pure Model MH-110, L. 12") and then dried to a target RH through NH-1. The
128 humid flow in the outer tube of NH-1 is a mixture of high-humidity air produced with a custom-built Gore-
129 Tex humidifier and heater (GTHH: TROPOS Model Di. 0.6", L. 11.8") and dry air in variable proportions.
130 To have a precise control of the aerosol RH, the flow rates of the humid and dry air are adjusted with a
131 proportional-integral-derivative (PID) system, including two mass flow controllers (MFC: MKS Model
132 MF1) and a RH sensor (Vaisala Model HMT330) downstream of NH-1.

133 The residence time is ~5.4 s in the NH-1 for both the deliquescence and the efflorescence mode. Many
134 groups have reported that the residence time of a few seconds is sufficient to reach equilibrium for
135 measuring hygroscopic growth or shrink of inorganic salts particles, e.g., ammonium sulfate and chloride
136 sodium (Chan and Chan, 2005; Duplissy et al., 2009; Lei et al., 2014, 2018; Giamarelou et al., 2018). More
137 specifically, Kerminen (1997) estimated the time for reaching the water equilibrium to be between 8×10^{-6}
138 s and 0.005 s for 100 nm nanoparticles at 90% RH at 25°C with accommodation coefficients from 0.001
139 to 1, respectively. In our study, we measured the inorganic aerosol nanoparticles with diameters from ~100
140 nm down to 6 nm, thus the equilibrium time should be even shorter as nanoparticle size decreases (Table.
141 S2). In NH-2, the residence time is ~0.07 s for the deliquescence of inorganic aerosol nanoparticles at very
142 high RH condition (~97% RH), which is much longer than the time estimated for phase transition by
143 Duplissy et al. (2009) (in the order of a few milliseconds) and Raoux et al. (2007) (in the order of a few
144 nanoseconds). In addition, we have tested a longer NH-2 (Perma Pure Model MH-110, L. 48") in the
145 efflorescence mode, and no significant difference in measured growth factors are found, indicating that the
146 residence time in NH-1 and NH-2 should be sufficient.



147 The number size distribution of the humidified nanoparticles is measured with a combination of the second
148 nano-DMA (nano-DMA2) and the ultrafine CPC. Similar to Biskos et al. (2016b), a multiple Nafion
149 humidifier (NH-3, Pure Model PD-100) is used in our nano-HTDMA system to rapidly adjust the RH of
150 the sheath flow of nano-DMA2. The sheath flow is fed into the outer tube of NH-3 to minimize its pressure
151 drop. The RH of humid flow in the inner tube of NH-3 is controlled with a similar PID system as that for
152 NH-1. A RH sensor (Vaisala Model HMT330) downstream of NH-3 is used to provide feedback to the PID
153 system. In our nano-HTDMA system, a dew point mirror (DPM: EDGE TECH Model MIRROR-99) is
154 placed in the excess flow line to measure the RH and temperature of excess flow of the nano-DMA2. During
155 the operation, the difference between sheath flow RH and aerosol flow RH has been maintained within
156 $\pm 1\%$ (see more details in Section 2.2).

157 The sheath flow is maintained to the set flow rate with a PID-controlled recirculation blower (RB:
158 AMETEK Series MINISPIRAL). Prior to every size scan, the sheath flow rate of nano-DMA2 is adjusted
159 by the PID system according to the measurement of a mass flow meter (MFM: TSI Series 4000) in the
160 sheath flow line. In order to minimize the pressure drop along the recirculating sheath flow loop, low flow
161 resistance MFM and hydrophobic filter (HF: Whatman Model 6702-3600) are used. A heat exchanger (HE,
162 Ebmpapst Model 4414FM) is installed downstream of the RB to minimize the temperature perturbation in
163 the sheath flow by the heat generated in the RB.

164 As aforementioned, temperature non-uniformity is the main contributor to the fluctuation of RH within
165 humidified DMA. Temperature difference within nano-DMA2 is unavoidable mainly due to temperature
166 difference between inner electrode and the rest of nano-DMA2 parts and/or the temperature difference
167 between aerosol and sheath flow (Duplissy et al., 2009; Bezantakos et al., 2016). As shown in Fig. 1, to
168 investigate and monitor the temperature difference within nano-DMA2 during measurements, a
169 temperature sensor (THERMO ELECTRON Model Pt100) is placed at the inlet of the sheath flow and the
170 temperature of sheath excess flow is monitored by the DPM. Note that, a DPM should be installed as close



171 as possible to the nano-DMA2 in the excess flow, which better represents the conditions inside the nano-
172 DMA2, such as temperature and RH (Wiedensohler et al., 2012). In addition, the temperature of aerosol
173 flow is monitored at the inlet of the aerosol flow of nano-DMA2.

174 Moreover, to maintain a stable environment that required for the growth factor measurements, nano-DMA2
175 with its sheath flow humidification system is placed in a well-insulated housing chamber (marked with
176 yellow dashed lines in Fig. 1). An air conditioner (Telemeter Electro Model TEK-1004-RR-24-IP55) is
177 installed inside the housing to maintain a constant temperature (292.15 ± 0.1 K), which is set to be ~ 1 K
178 lower than the constant laboratory temperature (293 K) in order to achieve high RH ($\sim 90\%$) inside nano-
179 DMA2.

180 **2.2 Calibration of nano-HTDMA**

181 The purpose of this study is to design and build a nano-HTDMA system that is able to measure the
182 hygroscopic properties of nanoparticles, especially in the sub-10 nm size range. A small perturbation in the
183 measurement conditions may lead to large biases in the results. Hence, to provide high quality
184 hygroscopicity measurements of nanoparticles, systematic calibration of the nano-HTDMA should be
185 conducted regularly to ensure the accuracy and stability of the measurement conditions. Table 1 lists the
186 possible sources of uncertainty, which could affect the performance of the HTDMAs. In our setup,
187 nanoparticle sizing, aerosol/sheath flow rates, the high voltage (HV) applied to nano-DMAs, RH sensors,
188 and temperature sensors are calibrated and verified independently.

189 Note that in the following, for calibration and/or checking of different parameters, the criteria and/or
190 standard that the nano-HTDMA system has to meet are listed mainly according to the suggestions from
191 Duplissy et al., (2009) and Wiedensohler et al. (2012), which are not specifically provided for accurately
192 measuring sizes or hygroscopic growth of sub-10 nm nanoparticles. Compared with these criteria, to
193 measure hygroscopic growth of sub-10 nm nanoparticles, we have achieved a better condition for our nano-



194 HTDMA system after comprehensive calibrations described as follows (more details about performance of
195 our system see section 3).

196 **2.2.1 Sizing accuracy**

197 For particle diameters higher than 100 nm, the verification of sizing accuracy of DMAs can be
198 accomplished by using certified particles of known sizes such as polystyrene latex (PSL) spheres (Hennig
199 et al., 2005; Mulholland et al., 2006; Duplissy et al., 2009; Wiedensohler et al., 2012, 2018). The particle
200 sizing of nano-DMA2 is checked with PSL by switching off the sheath flow and the HV supply of nano-
201 DMA1, which actually in this case does not function as a DMA, but rather a stainless-steel tube. Sizing
202 agreement between measured diameters and nominal diameters of PSL particles above 100 nm should be
203 within $\pm 3\%$ (Wiedensohler et al., 2012). After confirming the accurate sizing of nano-DMA2, the sizing
204 accuracy of nano-DMA1 can be in turn checked by the nano-DMA2 with a full scan of a certain size of
205 PSL selected by the nano-DMA1. Note that, it is important to check not only the sizing accuracy of both
206 DMAs, but also the sizing agreement between the nano-DMA1 and nano-DMA2. To achieve good
207 hygroscopicity measurements of nanoparticles, the sizing offset of the two DMAs should be within $\pm 2-3\%$
208 (Massling et al., 2011; Zhang et al., 2016).

209 For nanoparticles with diameters smaller than 100 nm, the sizing accuracy is, however, difficult to check
210 by using PSL nanoparticles. This is mainly because the size of residual material in the solution also peaks
211 around 20 – 30 nm (Fig. S2a), resulting in an asymmetric number size distribution of generated PSL
212 nanoparticles (Fig. S2b) (Wiedensohler et al., 2012). PSL nanoparticles with diameters below 20 nm are
213 not commercially available (<https://www.thermofisher.com/order/catalog/product/3020A>), making the
214 verification in this size range even impossible. Sizing accuracy of nanoparticles is critically determined by
215 sheath flow rates and HV applied to the nano-DMAs. However, unlike for the 100 nm nanoparticles, a $\pm 2-$
216 3% sizing offset between the two DMAs would be very difficult to maintain for nanoparticles with
217 diameters smaller than 20 nm. Thence, accurate calibrations of sheath flow rates and high voltage are crucial



218 for constraining the uncertainty associated with sizing of nanoparticles below 100 nm. The calibrations for
219 aerosol/sheath flow, DMA voltage, and sensors will be described in detail in the following Section 2.2.2-
220 2.2.5.

221 **2.2.2 Aerosol and sheath flow**

222 Sizing accuracy of a DMA directly depends on the accuracies of aerosol and sheath flow rates. The aerosol
223 flow rate at the inlet of the nano-DMA1 is checked by using a bubble flow meter (Gilian Model Gilibrator-
224 2). Wiedensohler et al. (2012) recommended that the measured aerosol flow rate should not deviate more
225 than 5% from the set flow rate during the measurements, otherwise one should check the flow rate of CPC
226 or if there is a leakage in the system. Details about leakage checking can be found in Birmili et al. (2016).

227 To calibrate the sheath flow, a verified MFM (TSI Series 4000) is placed in the recirculating sheath flow
228 close-loop upstream of the MFM. By applying a series of sheath flow rates, a calibration curve (flow rate
229 vs. MFM analogue output) can be obtained according to the reading of the reference MFM. Maximum
230 deviation of 2% from the sheath flow rate value of the reference MFM is recommended by Wiedensohler
231 et al. (2012), which can keep sizing accuracy of 200 nm PSL particles within $\pm 2\%$.

232 **2.2.3 DMA voltage**

233 The sizing of nano-DMAs is very sensitive to the accuracy and precision of the voltages applied, especially
234 when measuring nanoparticles in the sub-10 nm diameter range. A verified reference voltage meter with
235 voltage up to 1000 V (Prema Model 5000 DMM, accuracy 0.005%) is used to calibrate the HV supply of
236 the nano-DMAs (0-350 V). By setting a series of analogue voltage values, the HV applied to nano-DMA
237 can be calibrated according to the values shown in the reference voltage meter. For our nano-DMAs, sub-
238 10 nm in particle sizes correspond to voltage below 50 V. Thence, voltage calibration should be performed
239 with a higher resolution (smaller voltage interval) from 0 to 50 V (shown in the insert of Fig. 2).

240 **2.2.4 RH sensor**



241 One typical method to calibrate RH sensors in a HTDMA system is to measure the hygroscopic growth
242 factors of ammonium sulfate (Hennig et al., 2005), although the effects of shape factors, restructuring, and
243 impurities in the solutions may hamper a reliable RH calibration with this method (Duplissy et al., 2009).
244 Moreover, this indirect RH sensor calibration through measurement of the hygroscopic growth factors of
245 ammonium sulfate (usually with nanoparticle diameters around or above 100 nm) only calibrates the RH
246 values higher than the ERH of the pure salt. Calibration of RHs below ERH of ammonium sulfate is
247 important for the phase transition measurements. Most importantly, we are investigating the hygroscopic
248 growth factors of ammonium sulfate nanoparticles. Hence, using ammonium sulfate nanoparticles to
249 calibrate RH sensors in our system becomes invalid.

250 Therefore, we alternatively calibrate the RH sensors by using a DPM (EDGE TECH Model MIRROR-99),
251 which is recommended in several previous studies (Hennig et al., 2005; Duplissy et al., 2009; Biskos et al.,
252 2006a, b, 2007). In the calibration, the DPM and RH sensors should be kept in the well-insulated chamber
253 with constant laboratory conditions (e.g., flow rates, temperature, and pressure). By running the DPM and
254 all the other RH sensors in parallel at various RHs (5% to 90%), a calibration curve of the RHs measured
255 by the DPM against analogue voltages of RH sensor can be obtained.

256 **2.2.5 Temperature sensor**

257 Since all our temperature sensors and the high accurate DPM (EDGE TECH Model MIRROR-99) are
258 installed in the aforementioned well-insulated chamber and the chamber temperature is maintained with air
259 conditioner at about 292.15 ± 0.1 K, we calibrate the temperature sensors and corrected their systematic shift
260 by comparing the record of temperature sensors and the DPM by keeping them in parallel inside the
261 chamber over a 12-hour time period.

262 **2.3 Particle generation**



263 The experiments shown in this study were conducted using laboratory generated ammonium sulfate and
264 sodium sulfate nanoparticles. Nanoparticles with diameters of 6, 8, and 10 nm were generated by an
265 electrospray (AG: TSI Model 3480) with 1, 5, and 20 mM aqueous solution of ammonium sulfate and
266 sodium sulfate (Aldrich, 99.99%), respectively. The generated particles were then diluted and dried to RH
267 below 2% by mixing with dry and filtered N₂ (1 l/min) and CO₂ (0.1 l/min). The dried polydisperse aerosol
268 nanoparticles were subsequently neutralized by a Po²¹⁰ neutralizer. To avoid blocking the 25- μ m capillary
269 of the electrospray with high solution concentration, we used an atomizer (AG: TSI Model 3076) to
270 generate nanoparticles with diameters of 60-100 nm and 20nm with 0.05 and 0.001 wt% solution of
271 ammonium sulfate and sodium sulfate (Aldrich, 99.99%), respectively. Also, 100-nm PSL nanoparticles
272 were atomizing a PSL solution of mixing 3 drops of 100-nm PSL with 300 mL distilled and de-ionized
273 milli-Q water. The generated nanoparticles were subsequently dried to RH below 10% with a custom-built
274 Nafion dryer (ND: TROPOS Model ND.070) and then neutralized by a Kr⁸⁵ neutralizer.

275 The solutions used in our measurements were prepared with distilled and de-ionized milli-Q water
276 (resistivity of 18.2 M Ω cm at 298.15 K). Note that, for 100-60 nm and 20 nm, the solution concentration
277 was adjusted so that the sizes selected by the nano-DMA1 were always larger than the peak diameter of the
278 number size distribution of the generated nanoparticles to minimize the influence of the multiple charged
279 nanoparticles in hygroscopicity measurements. The influence of multiple charges on sub-10 nm particles
280 is expected to be very small, we, however, still used different concentrations so that the sizes selected by
281 the nano-DMA1 were always around the peak of the number size distribution of the generated nanoparticles
282 by the electrospray (Fig. S3). This is to ensure that we could have as many particles as possible to
283 compensate the strong loss of very small particles in the whole humidification systems.

284

285 **3 Results and discussion**

286 **3.1 Performance of the nano-HTDMA**



287 3.1.1 Sizing accuracy

288 In this section, we show the performance of our nano-HTDMA after a full calibration, including accuracy
289 and stability of the aerosol/sheath flow rates, the voltage applied to the nano-DMAs, and nanoparticle-
290 sizing accuracy. In our study, the sheath/aerosol flow rates and nano-DMA voltage supply have been
291 calibrated every day and every two weeks, respectively. The deviations of the measured aerosol/sheath flow
292 rates from the set-point values are less than $\pm 1\%$, which is lower than the maximum variation of 2%
293 recommended by Wiedensohler et al. (2012).

294 The voltage applied to the nano-DMAs (up to 350 V) is kept within $\pm 0.1\%$ around the set value shown in
295 the voltage meter. As shown in Fig. 3a, when test with 100-nm PSL nanoparticles, the average peak
296 diameter of scans from the nano-DMA2 is 100.4 nm, which matches well with the mean diameter of PSL
297 nanoparticles (100 ± 3 nm, Thermo Fisher Scientific Inc.). Afterwards, when using nano-DMA1 select 100
298 nm PSL, the scanned size distribution by nano-DMA2 has a peak diameter at 100.3 nm (Fig. 3b), indicating
299 a good sizing accuracy of the nano-DMA1 too.

300 After calibration, on average a $< 1.4\%$ sizing offset between the two nano-DMAs can be achieved for
301 ammonium sulfate nanoparticles with dry diameters of 100 nm, 60 nm and 20 nm (Fig. 3c, Fig.5, Table S3,
302 Fig. S4, and Fig. S5), which is much better than the 2-3% criteria recommended by Massling et al. (2011)
303 and Zhang et al. (2016). For sub-10 nm ammonium sulfate nanoparticles, our system has an average sizing
304 offset of $< 0.9\%$ for 10 and 8 nm particles and $\sim 1.4\%$ for 6 nm particles, respectively (Fig. 3d, Fig. 5, Table
305 S3, and Fig. S6). Note that, we also tested to calibrate the DMA voltage with a voltage meter with lower
306 accuracy of $\pm 1\%$, and the DMA voltages can only be kept within $\pm 1\%$ around the set value. In this way,
307 we found a much larger sizing offset for the sub-10 nm particles, i.e., 5.4% and 6.0% for 8 and 6 nm
308 ammonium sulfate nanoparticles, respectively. These results show that maintaining an accurate
309 sheath/aerosol flow (with $\pm 1\%$ around the set value) together with a careful voltage calibration (with $\pm 0.1\%$



310 around the set value, especially in low voltage range, i.e., <50 V for our system) is the key for accurate
311 sizing of sub-10 nm nanoparticles.

312 **3.1.2 Preventing pre-deliqescence in the deliqescence measurement mode**

313 Pre-deliqescence of dry nanoparticles in the deliqescence measurement mode is an important issue that
314 needs to be resolved in order to obtain accurate DRH (Biskos et al., 2006b; Duplissy et al., 2009;
315 Bezantakos et al., 2016; Hämeri et al., 2000). Since temperature and RH are closely linked and accurate
316 monitoring of these two quantities in the system are critical for nano-HTDMA measurements, we calibrated
317 all RH and T sensors regularly (every two weeks in this study). To prevent pre-deliqescence and optimize
318 the system, we have conducted three tests using ammonium sulfate nanoparticles with a dry diameter of
319 100 nm. In the first test, we regulated the RH of excess flow (RH_e) and made it equal to that of the aerosol
320 flow at the inlet of nano-DMA2 (RH_a), i.e., $RH_e=RH_a$, as done by previous HTDMA measurements, e.g.,
321 Villani et al. (2008). As shown in Fig. 4a, the measured growth factors of 100-nm ammonium sulfate are
322 in good agreement with predictions of the Extended Aerosol Inorganic Model (E-AIM; Clegg et al., 1998)
323 at RH above 80%. However, the ammonium sulfate nanoparticles deliquesce at 75% RH, which is
324 significantly lower than the expected DRH (80%, Tang and Munkelwitz (1994)). Since our RH sensors
325 were all well calibrated and the uncertainty of RH measurement is $\pm 1\%$, it is reasonable to hypothesize that
326 the RH upstream of nano-DMA2 has already reached the deliquesce RH of ammonium sulfate
327 nanoparticles. When these aerosol nanoparticles move downstream of the nano-DMA2, the RH decreases
328 back to 75%, which dehydrate the deliquesced ammonium sulfate nanoparticles. To avoid the pre-
329 deliqescence, Hämeri et al. (2001) has suggested to set RH_a to be 3-5% lower than RH_e . In the second test,
330 we have configured and regulated the system following this suggestion, i.e., $RH_e \geq RH_a + 3\%$. In this case,
331 the ammonium sulfate nanoparticles still deliquesce at 79% RH (Fig. 4b), even if RH_a is 6% lower than
332 RH_e .



333 Previous studies (Biskos et al., 2006b; Bezantakos et al., 2016) have shown that RH non-uniformities within
334 the nano-DMA2 can result in inaccurate measurements of phase transition and hygroscopic growth of
335 aerosol nanoparticles. One reason for RH non-uniformities within nano-DMA2 is that the sheath flow RH
336 is different from the aerosol flow RH at the inlet of the DMA (Hämeri et al., 2000, 2001). Another important
337 reason is the existence of temperature gradient within nano-DMA2 (Bezantakos et al., 2016). Hence, in the
338 third test, we moved the RH sensor from the excess flow downstream of nano-DMA2 to the sheath flow
339 upstream of nano-DMA2 and then regulated RH of sheath flow (RH_s) the same as RH_a (shown in Fig. 1),
340 i.e., $RH_s=RH_a$, as done by Kreidenweis et al. (2005), Biskos et al. (2006a, b), and Massling et al. (2011).
341 Note that to minimize the temperature gradient within the nano-DMA2 in our system so that nanoparticles
342 can undergo almost the same RH conditions, the nano-DMA2 with its sheath flow humidification system
343 has been placed in a well-insulated air-conditioned chamber. The air temperature inside the chamber can
344 be maintained at an almost constant level (292.15 ± 0.1 K). In addition, a heat exchanger was installed
345 downstream of the recirculation blower to minimize the temperature perturbation in the sheath flow by the
346 heat generated in the RB. Unlike previously reported by Bezantakos et al. (2016) that the RH at the outlet
347 was higher than that the inlet of the sheath air, we monitored that the sheath flow temperature at the inlet
348 of nano-DMA2 is slightly lower (less than ~ 0.2 K) than that at the outlet, i.e., the RH_s at the inlet of nano-
349 DMA2 is slightly higher ($\sim 1\%$) than the RH of the excess air at the outlet. It may be due to the heat produced
350 from the inner electrode of nano-DMA2, which we estimated to be ~ 0.08 W ($Q = mdTC_{p,k}$) by considering
351 the density and heating capacity of air, and aerosol and sheath air flow rate ($\rho=1.2041\text{kg/m}^3$; $C_p=$
352 $1.859\text{kJ/kg}^\circ\text{C}$; https://en.wikipedia.org/wiki/Density_of_air; [https://www.engineeringtoolbox.com/water-](https://www.engineeringtoolbox.com/water-vapor-d_979.html)
353 [vapor-d_979.html](https://www.engineeringtoolbox.com/water-vapor-d_979.html)). Although this temperature perturbation (less than ~ 0.2 K between the sheath flow at
354 the inlet and the excess flow at the outlet of the nano-DMA2) is larger than the ideal condition of less than
355 0.1 K that Duplissy et al. (2009) and Wiedensohler et al. (2012) suggested, our experimental results show
356 that a prompt phase transition can be still achieved. In this case, the measured DRH of ammonium sulfate
357 nanoparticles is almost at 80% (Fig. 4c and 4d).



358 **3.1.3 Prompt phase transition of ammonium sulfate**

359 Figure 5 and 6 show the normalized particle number size distributions measured by the nano-DMA2 in the
360 respective deliquescence and efflorescence measurement modes for ammonium sulfate nanoparticles with
361 dry mobility diameters of 20 nm, 10 nm, and 6 nm (see Fig. S4 for 100 nm, see Fig. S5 for 60 nm, see Fig.
362 S6 for 8 nm). In the deliquescence measurement mode (Fig. 5, Fig. S4a, and Fig. S5a), we observed the
363 similar double-mode phenomenon as reported by Mikhailov et al. (2004) and Biskos et al. (2006b, 2007).
364 For example, at 20 nm, there are two distinct intersecting modes of particle size distributions determined
365 by the nano-DMA2 in the RH range from 79% to 83% RH (around the DRH of ammonium sulfate). Biskos
366 et al. (2006b, 2007) attributed these two modes to the co-existence of solid and liquid phase nanoparticles
367 at RH close to the DRH of ammonium sulfate, due to the slight inhomogeneity of RH in the second nano-
368 DMA, i.e., some nanoparticles have already undergo deliquescence (liquid state) and some are not (solid).
369 This is evident through a double-mode log-normal fitting (red and blue modes in Fig. 5). Until RH ~82%,
370 the peak diameter of the red mode at 82% RH is similar to that at 11% RH, indicating that these
371 nanoparticles are still in a solid state. At 82% RH, a population of ammonium sulfate nanoparticles starts
372 to deliquesce and exists in a distinct mode with significant larger peak diameter (blue mode), although
373 majority of the nanoparticles remain solid (red mode). Further increase RH, the peak diameter of
374 normalized number size distribution of the blue mode increases, indicating the continuous growth the
375 nanoparticles after deliquescence. However, in our case the double-mode phenomenon was not observed
376 for 8 and 6 nm ammonium sulfate nanoparticles (Fig. 5 and Fig. S6a). To have a better estimation of DRH
377 when the double modes occurred, the peak diameter of the mode with larger number of nanoparticles was
378 chosen for growth factor calculation (Biskos et al., 2006b, 2007). For example, for 20 nm ammonium
379 sulfate nanoparticles, the peak diameters of normalized number size distribution of the red and blue modes
380 are used to calculate growth factor at RH between 79% to 83%, respectively.



381 For the efflorescence measurement mode, we adopted the approach of Biskos et al. (2006b) and used the
382 geometric standard deviation of number size distribution (sigma: σ) to quantify the diversity of the sizes of
383 nanoparticles. As shown in Fig. 6, Fig. S4b, Fig. S5b, and Fig. S6b, broadening of the normalized number
384 size distributions measured with nano-DMA2 was only observed for 20 nm ammonium sulfate
385 nanoparticles in the RH range from 33% to 30%. There, at RH higher than 33% or lower than 30%, σ stays
386 stably at 1.072. However, clear increases of σ (1.078-1.087) were observed for RH between 33% and 30%.
387 The normalized number size distributions in the RH range from 33% to 30% can be further resolved by
388 double-mode fit with fixed σ of 1.072 (the red and the blue mode in Fig. 6 for 20 nm). The ammonium
389 sulfate nanoparticles in the red mode at RH between 33% to 30% are in solid state because the peak diameter
390 of red mode is similar as that at 11% RH. However, within this RH range, the peak diameter of the blue
391 mode is significantly larger, indicating that these nanoparticles are still in liquid state. Further decreasing
392 RH (lower than 30%), only one mode has been observed and the peak diameter of the normalized number
393 size distribution almost unchanged as RH decreases (red mode in Fig. 6 for 20nm), which means that the
394 nanoparticles have been all in the solid state. Similar to the deliquescence measurement shown above and
395 in Fig. 5, the co-existence of solid and aqueous phase nanoparticles at RH 30-33% is also very likely to
396 stem from the slight heterogeneous RH in nano-DMA2 (Biskos et al., 2006b). To have a better estimation
397 of ERH when the broadening phenomenon exists, the peak diameter of the mode with larger number of
398 nanoparticles was used for growth factor calculation. After such data processing in both deliquescence and
399 efflorescence modes, we obtained prompt deliquescence and efflorescence of 6 to 100 nm ammonium
400 sulfate nanoparticles (more details in Section 3.1.4).

401 **3.1.4 Size-dependent hygroscopicity of ammonium sulfate nanoparticles**

402 Figure 7 shows the humidogram of ammonium sulfate nanoparticles measured by our nano-HTDMA
403 system in the size (dry diameter) range of 6-100 nm. The detailed comparison between our results and
404 Biskos et al. (2006b) during both deliquescence and efflorescence measurements are presented in Fig. 8a



405 and b (also Fig. S7). In general, our results are in a good agreement with the measurement results of Biskos
406 et al (2006) and the theoretical prediction by Cheng et al. (2015). First, there is a strong size dependence in
407 the hygroscopic growth factor of ammonium sulfate nanoparticles, and smaller ammonium sulfate
408 nanoparticles exhibit lower growth factor at a certain RH. For example, the difference of the growth factor
409 between 6 and 100 nm nanoparticles is up to 0.28 at 80% RH (Fig. S8a). Second, there is, however, no
410 significant size dependence in both DRH and ERH (Fig. S8b). For nanoparticles of different sizes (6-100
411 nm), the DRH and ERH of ammonium sulfate varies slightly from ~80-83% and ~30-34%, respectively.
412 This variation of the DRH and ERH along the size is much smaller for ammonium sulfate nanoparticles
413 than for sodium chloride (Biskos et al. 2006a, 2007).

414 Although our results in general agree well with Biskos et al. (2006b), the growth factors of 10, 8, and 6 nm
415 ammonium sulfate nanoparticles that we measured at high RH (i.e., > ~70%) are slightly lower (~0.02 in
416 growth factor) than that in Biskos et al. (2006b) in both deliquescence and efflorescence processes (Fig. 8b
417 and Fig. S7). We calculated the uncertainties of growth factor of 10-nm ammonium sulfate from 80% to

418 90% RH for our system and Biskos et al. (2006b) system by $\sqrt{\left(\left(g_f \frac{\sqrt{2}\epsilon_{Dp}}{D_p}\right)^2 + \left(\epsilon_{RH} \frac{dg_f}{dRH}\right)^2\right)}$ (Mochida

419 and Kawamura, (2004)). Here, ϵ_{Dp} , ϵ_{RH} , and g_f are uncertainty of particle mobility diameter, uncertainty
420 of relative humidity, and growth factor with respect to RH, respectively. The sizing offsets of our system
421 and Biskos et al. (2006b) for 10 nm ammonium sulfate are taken here as $\frac{\epsilon_{Dp}}{D_p}$ (see Table 1). As shown in the
422 insert of Fig. 8b, the discrepancies between the two systems are still within measurement uncertainty.

423 In addition, compared to Biskos et al. (2006b), our results show a similar re-structuring in deliquescence
424 mode at RH between about 20% to 75% for 100, and 60 nm ammonium sulfate nanoparticles (Fig 8c).
425 However, different than in Biskos et al. (2006b), we do not find re-structuring for smaller ammonium
426 sulfate nanoparticles (20, 10, 8, and 6 nm) at RH below deliquescence point (Fig. 8c and Fig. 8d). There
427 seems to be continues water adsorption and the adsorbed water layers (Romakkaniemi et al., 2001) become



428 significantly thicker when RH closer to the DRH (i.e., $RH > 70\%$). Note that, the ammonium sulfate
429 hygroscopic data from Biskos et al. (2006b) shown here are all generated by an electrospray, but in our
430 experiments, only the ammonium sulfate nanoparticles with diameters smaller than 20 nm (i.e., 10, 8, and
431 6 nm) were generated by an electrospray, while the larger nanoparticles (i.e., 20, 60, and 100 nm) were
432 generated by a atomizer. This means the different generation method and drying conditions may influence
433 the surface structure of the nanoparticles and thus their interaction with the adsorbed water layers (Iskandar
434 et al., 2003; Xin et al., 2019).

435 **3.2 Size-dependent hygroscopicity of sodium sulfate nanoparticles**

436 As a common constituent of atmospheric aerosol particles (Tang and Munkelwitz, 1993, 1994; Tang 1996;
437 Tang et al., 2007), hygroscopicity of sodium sulfate with diameters above 20 nm particles has been
438 investigated by a few groups (Tang et al., 2007; Xu and Schweiger, 1999; Hu et al., 2010). However, its
439 hygroscopic behavior in the sub-10 nm size range has not been investigated yet. In this study, we applied
440 our nano-HTDMA system to measure the hygroscopic growth factors, DRH, and ERH of sodium sulfate
441 nanoparticles with dry size from 20 nm down to 6 nm.

442 Figure 9 shows the measured size-resolved hygroscopic growth factors of sodium sulfate nanoparticles.
443 Different from the observations by Tang et al. (2007) using an electrodynamic balance (EDB), we observed
444 prompt deliquescence and efflorescence for both 20-nm and 6-nm sodium sulfate nanoparticles. Two
445 intersecting modes in the measured number size distribution of humidified sodium sulfate nanoparticles is
446 observed at RH close to the DRH (Fig. S9 and S10 in the Supplementary Information) and ERH, suggesting
447 an externally mixed of aqueous and solid nanoparticles. As shown in Sect. 3.1.3, a similar phenomenon is
448 also observed for ammonium sulfate, which could be attributed to the slight RH heterogeneities in nano-
449 DMA2, which makes only part of the nanoparticles deliquesce at RH close to the DRH, while the others
450 remain in solid state.



451 Together with the hygroscopic growth of 14-16 μm and 200-20 nm sodium sulfate measured previously by
452 Tang et al. (2007) and Hu et al. (2010), we show a strong size dependence in hygroscopic growth factors
453 of sodium sulfate nanoparticles (Fig. S11d). For example, at RH 84%, the hygroscopic growth factor of 6
454 nm sodium sulfate is only ~ 1.3 (in efflorescence mode), while the respective growth factors are about 1.5
455 and 1.8 for 20 nm and 14-16 μm particles. As shown in Fig. 9, E-AIM already agrees well with the
456 hygroscopic growth of micrometer particles (14-16 μm) without shape correction (DeCarlo et al., 2004),
457 i.e., shape factor (χ) of 1.0. However, to explain observation, a shape factor of ~ 1.16 and 1.26 would be
458 needed for 20 nm and 6 nm sodium sulfate nanoparticles, respectively.

459 There is no significant change in DRH between 14-16 μm ($\sim 84\%$) and 20 nm ($\sim 84\%$) sodium sulfate
460 particles (Fig. 9). This is consistent with Hu et al. (2010) where no change in DRH from 200 nm down to
461 20 nm ($\sim 82\%$, see Table 1 from Hu et al. (2010)) was observed. However, a significant increase of DRH
462 occurred when further decreasing particle diameters to 6 nm (DRH = $\sim 90\%$). The size dependence of ERH
463 is stronger than that of DRH, as there is already a clear increase of ERH from micrometer 14-16 μm ($\sim 57\%$)
464 to 20 nm ($\sim 62\%$) sodium sulfate particles. When further reducing the particle diameters to 6 nm, an almost
465 6% increase of DRH can be found, compared to the micrometer 14-16 μm particles (i.e., ERH increases
466 from 57 to 82%, respectively). The strong size-effect on the DRH and ERH of sodium chloride and on
467 hygroscopic growth factors of ammonium sulfate have been observed by Biskos et al. (2006a, b, 2007) and
468 theoretically studied and explained by Cheng et al. (2015). Owing to the strong non-ideality of aqueous
469 ammonium sulfate solution, the phase transition concentration (deliquescence and crystallization
470 concentration) of ammonium sulfate is much more sensitivity to the size changes from 60 nm to 6 nm than
471 that of sodium chloride, leading to the almost unchanged DRH and ERH of ammonium sulfate
472 nanoparticles (Cheng et al., 2015). Compared the three compounds, the size-dependent hygroscopicity of
473 sodium sulfate nanoparticles from 20 nm to 6 nm is similar to that of sodium chloride, but different to that
474 of ammonium sulfate, where no significant change in DRH and ERH was observed. However, in this size
475 range, the increase of the ERH and the decrease of growth factor upon decreasing size seems to be stronger



476 for sodium sulfate than sodium chloride, although no significant change in DRH was observed from
477 micrometer size particles down to 20 nm. As different hydrates of sodium sulfate may exist during the
478 deliquescence and efflorescence processes (Xu and Schweiger, 1999), to explain the underline mechanism
479 of the size dependent hygroscopicity of sodium sulfate particles can be challenging.

480

481 **4 Summary and Conclusion**

482 In this study, we presented our newly designed and self-assembled nano-HTDMA for measuring
483 hygroscopicity of nanoparticles in the sub-10 nm diameter size range. We also introduced the
484 comprehensive methods for system calibration and reported the performance of the system, focusing on the
485 sizing accuracy and preventing pre-deliqescence in the deliquescence measurement mode. By comparing
486 with previous studies on ammonium sulfate nanoparticles (Biskos et al., 2006b), we show that our system
487 is capable of providing high quality data of the hygroscopic behavior of sub-10 nm nanoparticles. We then
488 extended our measurements for sodium sulfate nanoparticles, of which size-dependent deliquescence and
489 efflorescence have been clearly observed for nanoparticles down to 6 nm in size, with similar behavior as
490 sodium chloride.

491 As we know, atmospheric aerosol particles consist of not only inorganic components, but also a vast number
492 of organic components existing in the atmosphere. However, their physico-chemical properties are still not
493 fully understood, especially when comes to the nano-scale and supersaturated concentration range. The
494 nano-HTDMA system can be directly applicable to explore the size dependence of aerosol nanoparticles.
495 Combing the multi-size measurements of hygroscopicity and the Differential Köhler Analyses (DKA,
496 Cheng et al., 2015) in nano size range, we will be able characterize and parameterize the water activity and
497 surface tension of different inorganic and organic systems. This will further help us to understand the
498 formation and transformation of aerosol nanoparticles in the atmosphere and their interaction with water
499 vapor.



500 **Data availability**

501 Readers who are interested in the data should contact Yafang Cheng (yafang.cheng@mpic.de).

502 **Acknowledgement**

503 This study was supported by the Max Planck Society (MPG) and Leibniz Society. T.L. acknowledges the
504 support from China Scholarship Council (CSC). Y.C. would like to acknowledge the Minerva Program of
505 MPG.

506 **Author contributions:** Y.C. and H.S. designed and led the study. N.M., T.T. and A. W. assembled the
507 basic HTDMA system. Y.C., H.S. and T.L. modified and advanced the basic system into the nano-HTDMA
508 for the purpose of measuring hygroscopic properties of aerosol nanoparticles in sub-10 nm size range at
509 MPIC. T.L. performed the experiments. J.H., N.M. and X.W. supported the experiments. All co-authors
510 discussed the results and commented on the manuscript. T.L. wrote the manuscript with input from all co-
511 authors.

512

513

514

515

516

517

518

519



520 **Reference**

- 521 Andreae, M. O., Afchine, A., Albrecht, R., Holanda, B. A., Artaxo, P., Barbosa, H. M. J., Borrmann, S.,
522 Cecchini, M. A., Costa, A., Dollner, M., Fütterer, D., Järvinen, E., Jurkat, T., Klimach, T., Konemann, T.,
523 Knote, C., Krämer, M., Krisna, T., Machado, L. A. T., Mertes, S., Minikin, A., Pöhlker, C., Pöhlker, M. L.,
524 Pöschl, U., Rosenfeld, D., Sauer, D., Schlager, H., Schnaiter, M., Schneider, J., Schulz, C., Spanu, A.,
525 Sperling, V. B., Voigt, C., Walser, A., Wang, J., Weinzierl, B., Wendisch, M., and Ziereis, H.: Aerosol
526 characteristics and particle production in the upper troposphere over the Amazon Basin, *Atmos. Chem.*
527 *Phys.*, 18, 921-961, 2018.
- 528 Badger, C. L., George, I., Griffiths, P. T., Braban, C. F., Cox, R. A., and Abbatt, J. P. D.: Phase transitions
529 and hygroscopic growth of aerosol particles containing humic acid and mixtures of humic acid and
530 ammonium sulphate, *Atmospheric Chemistry and Physics*, 6, 755-768, 2006.
- 531 Bezantakos, S., Huang, L., Barmounis, K., Martin, S. T., and Biskos, G.: Relative humidity non-
532 uniformities in Hygroscopic Tandem Differential Mobility Analyzer measurements, *Journal of Aerosol*
533 *Science*, 101, 1-9, 2016.
- 534 Birmili, W., Stratmann, F., Wiedensohler, A., Covert, D., M. Russell, L., and Berg, O.: Determination of
535 Differential Mobility Analyzer Transfer Functions Using Identical Instruments in Series, 1997.
- 536 Birmili, W., Weinhold, K., Rasch, F., Sonntag, A., Sun, J., Merkel, M., Wiedensohler, A., Bastian, S.,
537 Schladitz, A., Löschau, G., Cyrys, J., Pitz, M., Gu, J., Kusch, T., Flentje, H., Quass, U., Kaminski, H.,
538 Kuhlbusch, T. A. J., Meinhardt, F., and Fiebig, M.: Long-term observations of tropospheric particle number
539 size distributions and equivalent black carbon mass concentrations in the German Ultrafine Aerosol
540 Network (GUAN), 2016.



- 541 Biskos, G., Malinowski, A., Russell, L. M., Buseck, P. R., and Martin, S. T.: Nanosize Effect on the
542 Deliquescence and the Efflorescence of Sodium Chloride Particles, *Aerosol Science and Technology*, 40,
543 97-106, 2006a.
- 544 Biskos, G., Paulsen, D., Russell, L. M., Buseck, P. R., and Martin, S. T.: Prompt deliquescence and
545 efflorescence of aerosol nanoparticles, *Atmospheric Chemistry and Physics*, 6, 4633-4642, 2006b.
- 546 Biskos, G., Russell, L. M., Buseck, P. R., and Martin, S. T.: Nanosize effect on the hygroscopic growth
547 factor of aerosol particles, *Geophysical Research Letters*, 33, 2007.
- 548 Chan, M. N. and Chan, C. K.: Hygroscopic properties of two model humic-like substances and their
549 mixtures with inorganics of atmospheric importance, *Environmental Science & Technology*, 37, 5109-
550 5115, 2003.
- 551 Chan, M. N. and Chan, C. K.: Mass transfer effects in hygroscopic measurements of aerosol particles,
552 *Atmospheric Chemistry and Physics*, 2005.
- 553 Chan, M. N., Kreidenweis, S. M., and Chan, C. K.: Measurements of the Hygroscopic and Deliquescence
554 Properties of Organic Compounds of Different Solubilities in Water and Their Relationship with Cloud
555 Condensation Nuclei Activities, *Environmental Science & Technology*, 42, 3602-3608, 2008.
- 556 Chen, Da-Ren, David Y.H. Pui, and Stanley L. Kaufman.: Electrospinning of conducting liquids for
557 monodisperse aerosol generation in the 4 nm to 1.8 μm diameter range, *J. Aerosol Sci.*, 26: 963-977, 1995.
- 558 Cheng, Y., Su, H., Koop, T., Mikhailov, E., and Poschl, U.: Size dependence of phase transitions in aerosol
559 nanoparticles, *Nature communications*, 6, 5923, 2015.
- 560 Cheng, Y. F., Berghof, M., Garland, R. M., Wiedensohler, A., Wehner, B., Muller, T., Su, H., Zhang, Y.
561 H., Achtert, P., Nowak, A., Poschl, U., Zhu, T., Hu, M., and Zeng, L. M.: Influence of soot mixing state on



- 562 aerosol light absorption and single scattering albedo during air mass aging at a polluted regional site in
563 northeastern China, *Journal of Geophysical Research-Atmospheres*, 114, 2009.
- 564 Cheng, Y. F., Wiedensohler, A., Eichler, H., Heintzenberg, J., Tesche, M., Ansmann, A., Wendisch, M.,
565 Su, H., Althausen, D., Herrmann, H., Gnauk, T., Brüggemann, E., Hu, M., and Zhang, Y. H.: Relative
566 humidity dependence of aerosol optical properties and direct radiative forcing in the surface boundary layer
567 at Xinken in Pearl River Delta of China: An observation based numerical study, *Atmospheric Environment*,
568 42, 6373-6397, 2008.
- 569 Clegg, S. L., Brimblecombe, P., and Wexler, A. S.: Thermodynamic Model of the System $\text{H}^+ - \text{NH}_4^+ - \text{SO}_4^{2-}$
570 $- \text{NO}_3^- - \text{H}_2\text{O}$ at Tropospheric Temperatures, *The Journal of Physical Chemistry A*, 102, 2137-2154, 1998.
- 571 Collins, D. R., Cocker, D. R., Flagan, R. C., and Seinfeld, J. H.: The Scanning DMA Transfer Function,
572 *Aerosol Science and Technology*, 38, 833-850, 2004.
- 573 Cruz, C. N. and Pandis, S. N.: Deliquescence and Hygroscopic Growth of Mixed Inorganic–Organic
574 Atmospheric Aerosol, *Environmental Science & Technology*, 34, 4313-4319, 2000.
- 575 DeCarlo, P. F., Slowik, J. G., Worsnop, D. R., Davidovits, P., and Jimenez, J. L.: Particle Morphology and
576 Density Characterization by Combined Mobility and Aerodynamic Diameter Measurements. Part 1:
577 Theory, *Aerosol Science and Technology*, 38, 1185-1205, 2004.
- 578 Dong, J. L., Xiao, H. S., Zhao, L. J., and Zhang, Y.-H.: Spatially resolved Raman investigation on phase
579 separations of mixed $\text{Na}_2\text{SO}_4/\text{MgSO}_4$ droplets, 2009.
- 580 Dougle, P. G., Veefkind, J. P., and ten Brink, H. M.: Crystallisation of mixtures of ammonium nitrate,
581 ammonium sulphate and soot, *Journal of Aerosol Science*, 29, 375-386, 1998.
- 582 Dunne, E. M., Gordon, H., Kürten, A., Almeida, J., Duplissy, J., Williamson, C., Ortega, I. K., Pringle, K.
583 J., Adamov, A., Baltensperger, U., Barmet, P., Benduhn, F., Bianchi, F., Breitenlechner, M., Clarke, A.,



584 Curtius, J., Dommen, J., Donahue, N. M., Ehrhart, S., Flagan, R. C., Franchin, A., Guida, R., Hakala, J.,
585 Hansel, A., Heinritzi, M., Jokinen, T., Kangasluoma, J., Kirkby, J., Kulmala, M., Kupc, A., Lawler, M. J.,
586 Lehtipalo, K., Makhmutov, V., Mann, G., Mathot, S., Merikanto, J., Miettinen, P., Nenes, A., Onnela, A.,
587 Rap, A., Reddington, C. L. S., Riccobono, F., Richards, N. A. D., Rissanen, M. P., Rondo, L., Sarnela, N.,
588 Schobesberger, S., Sengupta, K., Simon, M., Sipilä, M., Smith, J. N., Stozkhov, Y., Tomé, A., Tröstl, J.,
589 Wagner, P. E., Wimmer, D., Winkler, P. M., Worsnop, D. R., and Carslaw, K. S.: Global atmospheric
590 particle formation from CERN CLOUD measurements, *Science*, 354, 1119-1124, 2016.

591 Duplissy, J., Gysel, M., S, S., Meyer, N., N, G., L, K., V, M., R, W., Martins dos Santos, S., C, G., Villani,
592 P., P, L., Sellegri, K., A, M., B. McFiggans, G., G, W., R, R., Dommen, J., Ristovski, Z., and Weingartner,
593 E.: Intercomparison study of six HTDMAs: results and general recommendations for HTDMA operation,
594 *Atmospheric Measurement Techniques*, 2. Pp, 363-378, 2009.

595 Ehn, M., Thornton, J. A., Kleist, E., Sipilä, M., Junninen, H., Pullinen, I., Springer, M., Rubach, F.,
596 Tillmann, R., Lee, B., Lopez-Hilfiker, F., Andres, S., Acir, I.-H., Rissanen, M., Jokinen, T., Schobesberger,
597 S., Kangasluoma, J., Kontkanen, J., Nieminen, T., Kurtén, T., Nielsen, L. B., Jørgensen, S., Kjaergaard, H.,
598 G., Canagaratna, M., Maso, M. D., Berndt, T., Petäjä, T., Wahner, A., Kerminen, V.-M., Kulmala, M.,
599 Worsnop, D. R., Wildt, J., and Mentel, T. F.: A large source of low-volatility secondary organic aerosol,
600 *Nature*, 506, 476, 2014.

601 Eichler, H., Cheng, Y., Birmili, W., Nowak, A., Wiedensohler, A., Brüggemann, E., Gnauk, T., Herrmann,
602 H., Althausen, D., Ansmann, A., Engelmann, R., Tesche, M., Wendisch, M., Zhang, Y. H., Hu, M., Liu, S.,
603 and Zeng, L.: Hygroscopic properties and extinction of aerosol particles at ambient relative humidity in
604 South-Eastern China, 2008.

605 Estillore, A. D., Morris, H. S., Or, V. W., Lee, H. D., Alves, M. R., Marciano, M. A., Laskina, O., Qin, Z.,
606 Tivanski, A. V., and Grassian, V. H.: Linking hygroscopicity and the surface microstructure of model



- 607 inorganic salts, simple and complex carbohydrates, and authentic sea spray aerosol particles, *Physical*
608 *Chemistry Chemical Physics*, 19, 21101-21111, 2017.
- 609 Fan, J., Rosenfeld, D., Zhang, Y., Giangrande, S. E., Li, Z., Machado, L. A. T., Martin, S. T., Yang, Y.,
610 Wang, J., Artaxo, P., Barbosa, H. M. J., Braga, R. C., Comstock, J. M., Feng, Z., Gao, W., Gomes, H. B.,
611 Mei, F., Pöhlker, C., Pöhlker, M. L., Pöschl, U., and de Souza, R. A. F.: Substantial convection and
612 precipitation enhancements by ultrafine aerosol particles, *Science*, 359, 411-418, 2018.
- 613 Gao, Y., Chen, S. B., and Yu, L. E.: Efflorescence Relative Humidity for Ammonium Sulfate Particles,
614 *The Journal of Physical Chemistry A*, 110, 7602-7608, 2006.
- 615 Ghorai, S., Wang, B., Tivanski, A., and Laskin, A.: Hygroscopic Properties of Internally Mixed Particles
616 Composed of NaCl and Water-Soluble Organic Acids, *Environmental Science & Technology*, 48, 2234-
617 2241, 2014.
- 618 Giamarelou, M., Smith, M., Papapanagiotou, E., Martin, S. T., and Biskos, G.: Hygroscopic properties of
619 potassium-halide nanoparticles, *Aerosol Science and Technology*, 52, 536-545, 2018.
- 620 Gysel, M., Weingartner, E., and Baltensperger, U.: Hygroscopicity of aerosol particles at low temperatures.
621 2. Theoretical and experimental hygroscopic properties of laboratory generated aerosols, *Environmental*
622 *Science & Technology*, 36, 63-68, 2002.
- 623 Hämeri, K., Laaksonen, A., Väkevä, M., and Suni, T.: Hygroscopic growth of ultrafine sodium chloride
624 particles, *Journal of Geophysical Research: Atmospheres*, 106, 20749-20757, 2001.
- 625 Hämeri, K., Väkevä, M., Hansson, H.-C., and Laaksonen, A.: Hygroscopic growth of ultrafine ammonium
626 sulfate aerosol measured using an ultrafine tandem differential mobility analyzer, *Journal of Geophysical*
627 *Research: Atmospheres*, 105, 22231-22242, 2000.



- 628 Hansson, H.-C., Rood, M. J., Koloutsou-Vakakis, S., Hämeri, K., Orsini, D., and Wiedensohler, A.: NaCl
629 Aerosol Particle Hygroscopicity Dependence on Mixing with Organic Compounds, *Journal of Atmospheric*
630 *Chemistry*, 31, 321-346, 1998.
- 631 Hennig, T., Massling, A., Brechtel, F. J., and Wiedensohler, A.: A tandem DMA for highly temperature-
632 stabilized hygroscopic particle growth measurements between 90 % and 98% relative humidity, *Journal of*
633 *Aerosol Science*, 36, 1210-1223, 2005.
- 634 Hong, J., Häkkinen, S. A. K., Paramonov, M., Äijälä, M., Hakala, J., Nieminen, T., Mikkilä, J., Prisle, N.
635 L., Kulmala, M., Riipinen, I., Bilde, M., Kerminen, V. M., and Petäjä, T.: Hygroscopicity, CCN and
636 volatility properties of submicron atmospheric aerosol in a boreal forest environment during the summer
637 of 2010, *Atmos. Chem. Phys.*, 14, 4733-4748, 2014.
- 638 Hong, J., Kim, J., Nieminen, T., Duplissy, J., Ehn, M., Äijälä, M., Hao, L. Q., Nie, W., Sarnela, N., Prisle,
639 N. L., Kulmala, M., Virtanen, A., Petäjä, T., and Kerminen, V. M.: Relating the hygroscopic properties of
640 submicron aerosol to both gas- and particle-phase chemical composition in a boreal forest environment,
641 *Atmos. Chem. Phys.*, 15, 11999-12009, 2015.
- 642 Hu, D., Qiao, L., Chen, J.-M., Ye, X., Yang, X., Cheng, T., and Fang, W.: Hygroscopicity of Inorganic
643 Aerosols: Size and Relative Humidity Effects on the Growth Factor, 2010.
- 644 Iskandar, F., Gradon, L., and Okuyama, K.: Control of the morphology of nanostructured particles prepared
645 by the spray drying of a nanoparticle sol, *Journal of Colloid and Interface Science*, 265, 296-303, 2003.
- 646 Kerminen, V. M.: The effects of particle chemical character and atmospheric processes on particle
647 hygroscopic properties, *Journal of Aerosol Science*, 28, 121-132, 1997.
- 648 Keskinen, H., Virtanen, A., Joutsensaari, J., Tsagkogeorgas, G., Duplissy, J., Schobesberger, S., Gysel, M.,
649 Riccobono, F., Slowik, J. G., Bianchi, F., Yli-Juuti, T., Lehtipalo, K., Rondo, L., Breitenlechner, M., Kupc,



650 A., Almeida, J., Amorim, A., Dunne, E. M., Downard, A. J., Ehrhart, S., Franchin, A., Kajos, M. K., Kirkby,
651 J., Kürten, A., Nieminen, T., Makhmutov, V., Mathot, S., Miettinen, P., Onnela, A., Petäjä, T., Praplan, A.,
652 Santos, F. D., Schallhart, S., Sipilä, M., Stozhkov, Y., Tomé, A., Vaattovaara, P., Wimmer, D., Prevot, A.,
653 Dommen, J., Donahue, N. M., Flagan, R. C., Weingartner, E., Viisanen, Y., Riipinen, I., Hansel, A.,
654 Curtius, J., Kulmala, M., Worsnop, D. R., Baltensperger, U., Wex, H., Stratmann, F., and Laaksonen, A.:
655 Evolution of particle composition in CLOUD nucleation experiments, *Atmos. Chem. Phys.*, 13, 5587-5600,
656 2013.

657 Kim, J., Ahlm, L., Yli-Juuti, T., Lawler, M., Keskinen, H., Tröstl, J., Schobesberger, S., Duplissy, J.,
658 Amorim, A., Bianchi, F., Donahue, N. M., Flagan, R. C., Hakala, J., Heinritzi, M., Jokinen, T., Kürten, A.,
659 Laaksonen, A., Lehtipalo, K., Miettinen, P., Petäjä, T., Rissanen, M. P., Rondo, L., Sengupta, K., Simon,
660 M., Tomé, A., Williamson, C., Wimmer, D., Winkler, P. M., Ehrhart, S., Ye, P., Kirkby, J., Curtius, J.,
661 Baltensperger, U., Kulmala, M., Lehtinen, K. E. J., Smith, J. N., Riipinen, I., and Virtanen, A.:
662 Hygroscopicity of nanoparticles produced from homogeneous nucleation in the CLOUD experiments,
663 *Atmos. Chem. Phys.*, 16, 293-304, 2016.

664 Kirkby, J., Curtius, J., Almeida, J., Dunne, E., Duplissy, J., Ehrhart, S., Franchin, A., Gagné, S., Ickes, L.,
665 Kürten, A., Kupc, A., Metzger, A., Riccobono, F., Rondo, L., Schobesberger, S., Tsagkogeorgas, G.,
666 Wimmer, D., Amorim, A., Bianchi, F., Breitenlechner, M., David, A., Dommen, J., Downard, A., Ehn, M.,
667 Flagan, R. C., Haider, S., Hansel, A., Hauser, D., Jud, W., Junninen, H., Kreissl, F., Kvashin, A.,
668 Laaksonen, A., Lehtipalo, K., Lima, J., Lovejoy, E. R., Makhmutov, V., Mathot, S., Mikkilä, J., Minginette,
669 P., Mogo, S., Nieminen, T., Onnela, A., Pereira, P., Petäjä, T., Schnitzhofer, R., Seinfeld, J. H., Sipilä, M.,
670 Stozhkov, Y., Stratmann, F., Tomé, A., Vanhanen, J., Viisanen, Y., Vrtala, A., Wagner, P. E., Walther, H.,
671 Weingartner, E., Wex, H., Winkler, P. M., Carslaw, K. S., Worsnop, D. R., Baltensperger, U., and Kulmala,
672 M.: Role of sulphuric acid, ammonia and galactic cosmic rays in atmospheric aerosol nucleation, *Nature*,
673 476, 429-433, 2011.



- 674 Köhler, H.: The nucleus in and the growth of hygroscopic droplets, *Transactions of the Faraday Society*,
675 32, 1152-1161, 1936.
- 676 Kreidenweis, S. M., Koehler, K., DeMott, P. J., Prenni, A. J., Carrico, C., and Ervens, B.: Water activity
677 and activation diameters from hygroscopicity data - Part I: Theory and application to inorganic salts,
678 *Atmospheric Chemistry and Physics*, 5, 1357-1370, 2005.
- 679 Lei, T., Zuend, A., Cheng, Y., Su, H., Wang, W., and Ge, M.: Hygroscopicity of organic surrogate
680 compounds from biomass burning and their effect on the efflorescence of ammonium sulfate in mixed
681 aerosol particles, *Atmos. Chem. Phys.*, 18, 1045-1064, 2018.
- 682 Lei, T., Zuend, A., Wang, W. G., Zhang, Y. H., and Ge, M. F.: Hygroscopicity of organic compounds from
683 biomass burning and their influence on the water uptake of mixed organic ammonium sulfate aerosols,
684 *Atmos. Chem. Phys.*, 14, 11165-11183, 2014.
- 685 Lihavainen, H., Kerminen, V.-M., Komppula, M., Hatakka, J., Aaltonen, V., Kulmala, M., and Viisanen,
686 Y.: Production of “potential” cloud condensation nuclei associated with atmospheric new-particle
687 formation in northern Finland, *Journal of Geophysical Research: Atmospheres*, 108, 2003.
- 688 Martin, S. T.: Phase Transitions of Aqueous Atmospheric Particles, *Chemical Reviews*, 100, 3403-3454,
689 2000.
- 690 Massling, A., Niedermeier, N., Hennig, T., Fors, E. O., Swietlicki, E., Ehn, M., Hämeri, K., Villani, P., Laj,
691 P., Good, N., McFiggans, G., and Wiedensohler, A.: Results and recommendations from an
692 intercomparison of six Hygroscopicity-TDMA systems, *Atmos. Meas. Tech.*, 4, 485-497, 2011.
- 693 McMurry, P. H.: A review of atmospheric aerosol measurements, *Atmospheric Environment*, 34, 1959-
694 1999, 2000.



- 695 Mikhailov, E., Vlasenko, S., Martin, S. T., Koop, T., and Poschl, U.: Amorphous and crystalline aerosol
696 particles interacting with water vapor: conceptual framework and experimental evidence for restructuring,
697 phase transitions and kinetic limitations, *Atmospheric Chemistry and Physics*, 9, 9491-9522, 2009.
- 698 Mikhailov, E., Vlasenko, S., Niessner, R., and Poschl, U.: Interaction of aerosol particles composed of
699 protein and salts with water vapor: hygroscopic growth and microstructural rearrangement, *Atmospheric*
700 *Chemistry and Physics*, 4, 323-350, 2004.
- 701 Mikhailov, E., Vlasenko, S., Rose, D., and Pöschl, U.: Mass-based hygroscopicity parameter interaction
702 model and measurement of atmospheric aerosol water uptake, *Atmos. Chem. Phys.*, 13, 717-740, 2013.
- 703 Mikhailov, E. F. and Vlasenko, S. S.: High humidity tandem differential mobility analyzer for accurate
704 determination of aerosol hygroscopic growth, microstructure and activity coefficients over a wide range of
705 relative humidity, *Atmos. Meas. Tech. Discuss.*, <https://doi.org/10.5194/amt-2019-478>, in review, 2019.
- 706 Mikhailov, E. F., Vlasenko, S. S., and Ryshkevich, T. I.: Influence of chemical composition and
707 microstructure on the hygroscopic growth of pyrogenic aerosol, *Izvestiya, Atmospheric and Oceanic*
708 *Physics*, 44, 416-431, 2008.
- 709 Mirabel, P., Reiss, H., and Bowles, R. K.: A theory for the deliquescence of small particles, *The Journal of*
710 *Chemical Physics*, 113, 8200-8205, 2000.
- 711 Mochida, M. and Kawamura, K.: Hygroscopic properties of levoglucosan and related organic compounds
712 characteristic to biomass burning aerosol particles, *Journal of Geophysical Research-Atmospheres*, 109,
713 2004.
- 714 Mulholland, G. W., Donnelly, M. K., Hagwood, C. R., Kukuck, S. R., Hackley, V. A., and Pui, D. Y. H.:
715 Measurement of 100 nm and 60 nm Particle Standards by Differential Mobility Analysis, *Journal of*
716 *Research of the National Institute of Standards and Technology*, 111, 257-312, 2006.



- 717 Park, K., Kim, J.-S., and Miller, A. L.: A study on effects of size and structure on hygroscopicity of
718 nanoparticles using a tandem differential mobility analyzer and TEM, *Journal of Nanoparticle Research*,
719 11, 175-183, 2009.
- 720 Peng, C., Chow, A. H. L., and Chan, C. K.: Hygroscopic Study of Glucose, Citric Acid, and Sorbitol Using
721 an Electrodynamic Balance: Comparison with UNIFAC Predictions, *Aerosol Science and Technology*, 35,
722 753-758, 2001.
- 723 Pope, F. D., Dennis-Smith, B. J., Griffiths, P. T., Clegg, S. L., and Cox, R. A.: Studies of Single Aerosol
724 Particles Containing Malonic Acid, Glutaric Acid, and Their Mixtures with Sodium Chloride. I.
725 Hygroscopic Growth, *The Journal of Physical Chemistry A*, 114, 5335-5341, 2010.
- 726 Pruppacher, H. R. & Klett, J. D: *Microphysics of clouds and precipitation*, Kluwer Academic Publishers,
727 1997.
- 728 Rader, D. J. and McMurry, P. H.: Application of the tandem differential mobility analyzer to studies of
729 droplet growth or evaporation, *Journal of Aerosol Science*, 17, 771-787, 1986.
- 730 Raoux, S., Rettner, C. T., Jordan-Sweet, J. L., Kellock, A. J., Topuria, T., Rice, P. M., and Miller, D. C.:
731 Direct observation of amorphous to crystalline phase transitions in nanoparticle arrays of phase change
732 materials, *Journal of Applied Physics*, 102, 094305, 2007.
- 733 Reid, J. P., Dennis-Smith, B. J., Kwamena, N.-O. A., Miles, R. E. H., Hanford, K. L., and Homer, C. J.:
734 The morphology of aerosol particles consisting of hydrophobic and hydrophilic phases: hydrocarbons,
735 alcohols and fatty acids as the hydrophobic component, *Physical Chemistry Chemical Physics*, 13, 15559-
736 15572, 2011.
- 737 Richardson, C. B. and Spann, J.: Measurement of Water Cycle in a Levitated Ammonium Sulfate Particles,
738 1984.



- 739 Rickards, A. M. J., Miles, R. E. H., Davies, J. F., Marshall, F. H., and Reid, J. P.: Measurements of the
740 Sensitivity of Aerosol Hygroscopicity and the κ Parameter to the O/C Ratio, *The Journal of Physical*
741 *Chemistry A*, 117, 14120-14131, 2013.
- 742 Romakkaniemi, S., Hämeri, K., Väkevä, M., and Laaksonen, A.: Adsorption of Water on 8–15 nm NaCl
743 and (NH₄)₂SO₄ Aerosols Measured Using an Ultrafine Tandem Differential Mobility Analyzer, *The*
744 *Journal of Physical Chemistry A*, 105, 8183-8188, 2001.
- 745 Russell, L. M. and Ming, Y.: Deliquescence of small particles, *Journal of Chemical Physics*, 116, 311-321,
746 2002.
- 747 Sakurai, H., A. Fink, M., H. McMurry, P., Mauldin, R., F. Moore, K., N. Smith, J., and Eisele, F.:
748 Hygroscopicity and volatility of 4–10 nm particles during summertime atmospheric nucleation events in
749 urban Atlanta, 2005.
- 750 Seinfeld, J. H., and S. N. Pandis: *Atmospheric Chemistry and Physics: From Air Pollution to Climate*
751 *Change*, 2nd ed., John Wiley, New York, 2006.
- 752 Sihto, S. L., Mikkilä, J., Vanhanen, J., Ehn, M., Liao, L., Lehtipalo, K., Aalto, P. P., Duplissy, J., Petäjä,
753 T., Kerminen, V. M., Boy, M., and Kulmala, M.: Seasonal variation of CCN concentrations and aerosol
754 activation properties in boreal forest, *Atmos. Chem. Phys.*, 11, 13269-13285, 2011.
- 755 Stock, M., Cheng, Y. F., Birmili, W., Massling, A., Wehner, B., Müller, T., Leinert, S., Kalivitis, N.,
756 Mihalopoulos, N., and Wiedensohler, A.: Hygroscopic properties of atmospheric aerosol particles over the
757 Eastern Mediterranean: implications for regional direct radiative forcing under clean and polluted
758 conditions, *Atmos. Chem. Phys.*, 11, 4251-4271, 2011.
- 759 Su, H., Rose, D., Cheng, Y. F., Gunthe, S. S., Massling, A., Stock, M., Wiedensohler, A., Andreae, M. O.,
760 and Pöschl, U.: Hygroscopicity distribution concept for measurement data analysis and modeling of aerosol



- 761 particle mixing state with regard to hygroscopic growth and CCN activation, *Atmos. Chem. Phys.*, 10,
762 7489-7503, 2010.
- 763 Tang, I. N.: Chemical and size effects of hygroscopic aerosols on light scattering coefficients, *Journal of*
764 *Geophysical Research: Atmospheres*, 101, 19245-19250, 1996.
- 765 Tang, I. N., Fung, K. H., Imre, D. G., and Munkelwitz, H. R.: Phase Transformation and Metastability of
766 Hygroscopic Microparticles, *Aerosol Science and Technology*, 23, 443-453, 2007.
- 767 Tang, I. N. and Munkelwitz, H. R.: Composition and temperature dependence of the deliquescence
768 properties of hygroscopic aerosols, *Atmospheric Environment. Part A. General Topics*, 27, 467-473, 1993.
- 769 Tang, I. N. and Munkelwitz, H. R.: Water activities, densities, and refractive indices of aqueous sulfates
770 and sodium nitrate droplets of atmospheric importance, *Journal of Geophysical Research: Atmospheres*,
771 99, 18801-18808, 1994.
- 772 Tang, M., Chan, C. K., Li, Y. J., Su, H., Ma, Q., Wu, Z., Zhang, G., Wang, Z., Ge, M., Hu, M., He, H., and
773 Wang, X.: A review of experimental techniques for aerosol hygroscopicity studies, *Atmos. Chem. Phys.*,
774 19, 12631-12686, 2019.
- 775 Topping, D., McFiggans, G., and Coe, H.: A curved multi-component aerosol hygroscopicity model
776 framework: Part 1–Inorganic compounds, *Atmospheric Chemistry and Physics*, 5, 1205-1222, 2005.
- 777 Villani, P., Picard, D., Michaud, V., Laj, P., and Wiedensohler, A.: Design and Validation of a Volatility
778 Hygroscopic Tandem Differential Mobility Analyzer (VH-TDMA) to Characterize the Relationships
779 Between the Thermal and Hygroscopic Properties of Atmospheric Aerosol Particles, *Aerosol Science and*
780 *Technology*, 42, 729-741, 2008.
- 781 Vlasenko, S. S., Su, H., Pöschl, U., Andreae, M. O., and Mikhailov, E. F.: Tandem configuration of
782 differential mobility and centrifugal particle mass analysers for investigating aerosol hygroscopic
783 properties, *Atmos. Meas. Tech.*, 10, 1269-1280, 2017.



- 784 Wang, J., Krejci, R., Giangrande, S., Kuang, C., Barbosa, H. M. J., Brito, J., Carbone, S., Chi, X.,
785 Comstock, J., Ditas, F., Lavric, J., Manninen, H. E., Mei, F., Moran-Zuloaga, D., Pöhlker, C., Pöhlker, M.
786 L., Saturno, J., Schmid, B., Souza, R. A. F., Springston, S. R., Tomlinson, J. M., Toto, T., Walter, D.,
787 Wimmer, D., Smith, J. N., Kulmala, M., Machado, L. A. T., Artaxo, P., Andreae, M. O., Petäjä, T., and
788 Martin, S. T.: Amazon boundary layer aerosol concentration sustained by vertical transport during rainfall,
789 *Nature*, 539, 416, 2016.
- 790 Wang, L., Khalizov, A. F., Zheng, J., Xu, W., Ma, Y., Lal, V., and Zhang, R.: Atmospheric nanoparticles
791 formed from heterogeneous reactions of organics, *Nature Geoscience*, 3, 238, 2010.
- 792 Wang, X., Ma, N., Lei, T., Größ, J., Li, G., Liu, F., Meusel, H., Mikhailov, E., Wiedensohler, A., and Su,
793 H.: Effective density and hygroscopicity of protein particles generated with spray-drying process, *Journal*
794 *of Aerosol Science*, 137, 105441, 2019.
- 795 Wang, Z., Su, H., Wang, X., Ma, N., Wiedensohler, A., Pöschl, U., and Cheng, Y.: Scanning
796 supersaturation condensation particle counter applied as a nano-CCN counter for size-resolved analysis of
797 the hygroscopicity and chemical composition of nanoparticles, *Atmos. Meas. Tech.*, 8, 2161-2172,
798 <https://doi.org/10.5194/amt-8-2161-2015>, 2015.
- 799 Wiedensohler, A., Birmili, W., Nowak, A., Sonntag, A., Weinhold, K., Merkel, M., Wehner, B., Tuch, T.,
800 Pfeifer, S., Fiebig, M., Fjåraa, A. M., Asmi, E., Sellegri, K., Depuy, R., Venzac, H., Villani, P., Laj, P.,
801 Aalto, P., Ogren, J. A., Swietlicki, E., Williams, P., Roldin, P., Quincey, P., Hüglin, C., Fierz-
802 Schmidhauser, R., Gysel, M., Weingartner, E., Riccobono, F., Santos, S., Gruning, C., Faloon, K.,
803 Beddows, D., Harrison, R., Monahan, C., Jennings, S. G., O'Dowd, C. D., Marinoni, A., Horn, H. G., Keck,
804 L., Jiang, J., Scheckman, J., McMurry, P. H., Deng, Z., Zhao, C. S., Moerman, M., Henzing, B., de Leeuw,
805 G., Löschau, G., and Bastian, S.: Mobility particle size spectrometers: harmonization of technical standards
806 and data structure to facilitate high quality long-term observations of atmospheric particle number size
807 distributions, *Atmos. Meas. Tech.*, 5, 657-685, 2012.



- 808 Wiedensohler, A., Cheng, Y. F., Nowak, A., Wehner, B., Achtert, P., Berghof, M., Birmili, W., Wu, Z. J.,
809 Hu, M., Zhu, T., Takegawa, N., Kita, K., Kondo, Y., Lou, S. R., Hofzumahaus, A., Holland, F., Wahner,
810 A., Gunthe, S. S., Rose, D., Su, H., and Pöschl, U.: Rapid aerosol particle growth and increase of cloud
811 condensation nucleus activity by secondary aerosol formation and condensation: A case study for regional
812 air pollution in northeastern China, *Journal of Geophysical Research: Atmospheres*, 114, 2009.
- 813 Wiedensohler, A., Wiesner, A., Weinhold, K., Birmili, W., Hermann, M., Merkel, M., Müller, T., Pfeifer,
814 S., Schmidt, A., Tuch, T., Velarde, F., Quincey, P., Seeger, S., and Nowak, A.: Mobility particle size
815 spectrometers: Calibration procedures and measurement uncertainties, *Aerosol Science and Technology*,
816 52, 146-164, 2018.
- 817 Wise, M. E., Surratt, J. D., Curtis, D. B., Shilling, J. E., and Tolbert, M. A.: Hygroscopic growth of
818 ammonium sulfate/dicarboxylic acids, *Journal of Geophysical Research-Atmospheres*, 108, 2003.
- 819 Wu, Z. J., Nowak, A., Poulain, L., Herrmann, H., and Wiedensohler, A.: Hygroscopic behavior of
820 atmospherically relevant water-soluble carboxylic salts and their influence on the water uptake of
821 ammonium sulfate, *Atmos. Chem. Phys.*, 11, 12617-12626, 2011.
- 822 Xu, B. and Schweiger, G.: In-situ Raman observation of phase transformation of Na₂SO₄ during the
823 hydration/dehydration cycles on single levitated microparticle, 1999.
- 824 You, Y., Renbaum-Wolff, L., and Bertram, A. K.: Liquid–liquid phase separation in particles containing
825 organics mixed with ammonium sulfate, ammonium bisulfate, ammonium nitrate or sodium chloride,
826 *Atmos. Chem. Phys.*, 13, 11723-11734, 2013.
- 827 Zawadowicz, M. A., Proud, S. R., Seppäläinen, S. S., and Cziczo, D. J.: Hygroscopic and phase separation
828 properties of ammonium sulfate/organics/water ternary solutions, *Atmos. Chem. Phys.*, 15, 8975-8986,
829 2015.



830 Zhang, S. L., Ma, N., Kecorius, S., Wang, P. C., Hu, M., Wang, Z. B., Größ, J., Wu, Z. J., and Wiedensohler,
831 A.: Mixing state of atmospheric particles over the North China Plain, *Atmospheric Environment*, 125, 152-
832 164, 2016.

833 Zhao, L.-J., Zhang, Y.-H., Wei, Z.-F., Cheng, H., and Li, X.-H.: Magnesium Sulfate Aerosols Studied by
834 FTIR Spectroscopy: Hygroscopic Properties, Supersaturated Structures, and Implications for Seawater
835 Aerosols, *The Journal of Physical Chemistry A*, 110, 951-958, 2006.

836

837

838

839

840

841

842

843

844

845

846

847

848

849



850 **Tables**

851 **Table 1.** Accuracy, precision and sources of uncertainty associated with HTDMA measurements.

	Biskos et al. (2006b)	Hämeri et al. (2000)	Nano-HTDMA (This study)
DMA System			
Type of DMA1 & DMA2	TSI nano-DMAs	Hauke-type DMAs	Vienna-type short DMAs
Accuracy of aerosol flow in DMA2	±1% (0.3-1.5 l/min)	-	±1% (1.5 l/min)
Accuracy of sheath flow in DMA2	±1% (5-15 l/min)	-	±1% (10 l/min)
Accuracy of DMA voltage	±0.1% (0-500V)	-	±0.1% (0-350V)
Sizing accuracy of DMA2 using PSL	3%	-	0.4% (100-nm PSL)
Sizing agreement between DMAs using ammonium sulfate	3.1% (10 nm) ^a	±1% ^b	0.6% (100 nm) ^c 0.5% (60 nm) ^c 1.4% (20 nm) ^c 0.9% (10 nm) ^c -0.2% (8 nm) ^c 1.4% (6 nm) ^c
Precision of particle-sizing	<2%	-	<2% (6-200 nm) ^d



Humidification System			
Type of RH sensor	RH sensors (Omega Model HX93AV)	Dew point mirror (GE) RH sensors (Vaisala Humitter model 50Y)	Dew point mirror (Edge) RH sensors (Vaisala model HMT 330)
Accuracy of RH sensors (0-90% RH)	±2.5% RH	±3% RH ^e	±1% (RH sensor)
Position of the probe in the system	Inlet of DMA2 (RH _a sensor ^f , RH _s sensor ^g)	Inlet of DMA2 (RH _a sensor) & excess air (RH _s sensor, dew point mirror)	Inlet of DMA2 (RH _a sensor, RH _s sensor) & excess air (dew point mirror)
RH setting	RH _a =RH _s	RH _s ≥ RH _a +3%	RH _a =RH _s
Temperature Control System			
Temperature control type	Thermally isolated environment (humidification+DMA2) ^h	Thermally isolated environment (DMA2)	Box T regulated (humidification+DMA2)
Difference in T between inlet and outlet of DMA2	-	-	<0.2°C

852 ^aNot reported.

853 ^a According to the scans of the second DMA for the hygroscopic growth of 10 nm ammonium sulfate and the growth factors at different RHs provided by Biskos et al.
 854 (2006b), we retrieved an average sizing offset of Biskos et al. (2006b) system to be ~3.1% at 10 nm (see SI, S1).

855 ^b Size range not given.

856 ^c See Table S2 in supporting information.

857 ^d Value calculated according to the relative standard derivation.

858 ^e From Vaisala Humitter model 50Y manual.

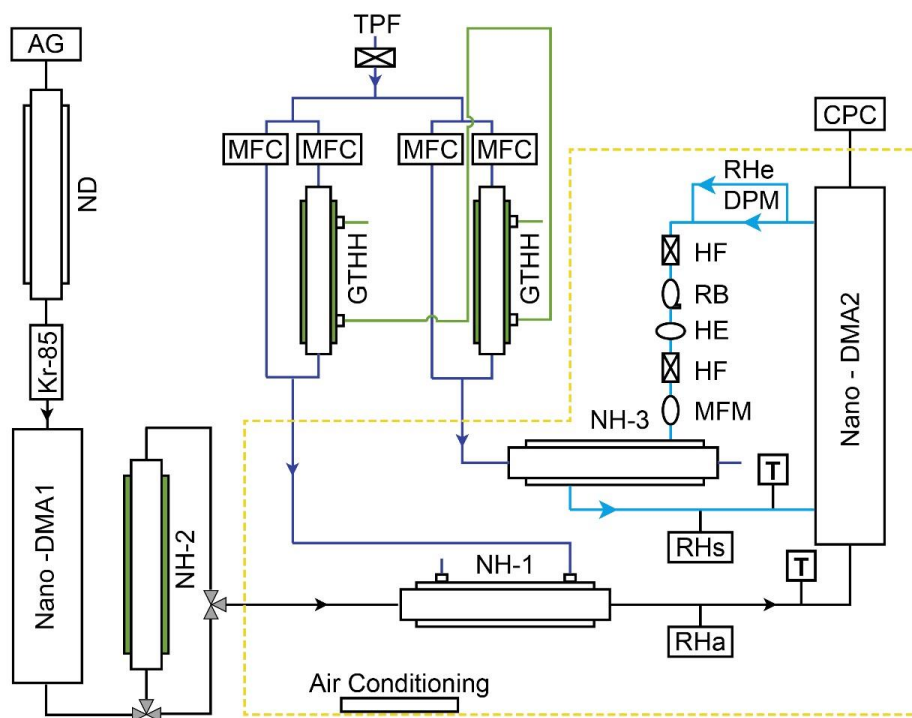
859 ^f RH_a: the RH of aerosol flow.

860 ^g RH_s: the RH of sheath flow.

861 ^h Bezantakos et al. (2016).



862 **Figures**



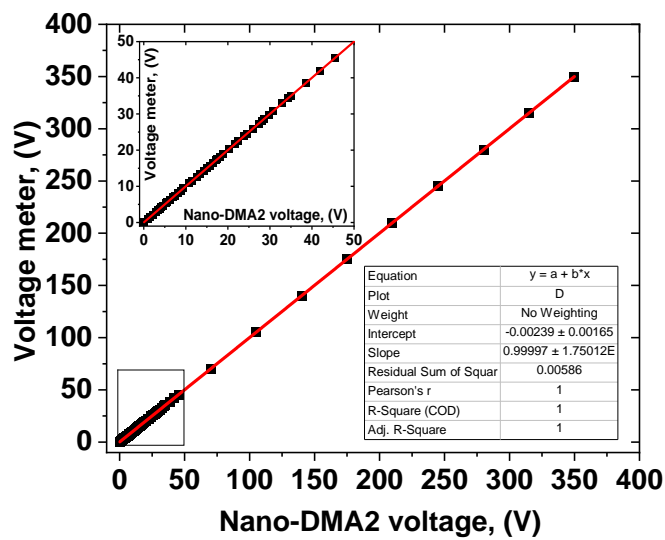
863

864 **Figure 1.** Experimental setup of the nano-HTDMA. Here, AG: aerosol generator (aerosol atomizer or electro spray);
865 ND: nafion dryer; Kr-85: Krypton source aerosol neutralizer; Nano-DMA: nano differential mobility analyzer; TPF:
866 total particle filter; HF: hydrophobic filter; MFC: mass flow controller; MFM: mass flow meter; RB: recirculation
867 blower; DPM: dew point mirror; GTHH: Gore-Tex humidifier and heater; NH: nafion humidifier; HE: heat exchanger;
868 CPC: condensation particle counter; Black line: aerosol line; Blue line: sheath line; Royal blue line: humidified air;
869 Green line: MilliQ water (resistivity of 18.2 MΩ cm at 298.15 K). RH_a and RH_s (measured by RH sensors) represent
870 the RH of aerosol and sheath flow in the inlet of nano-DMA2, respectively. RH_e (measured by dew point) represents
871 the RH of excess air. T represent the temperature of aerosol and sheath flow in the inlet of nano-DMA2, respectively.

872

873

874



875

876

Figure 2. An example of voltage calibration of the nano-DMA2.

877

878

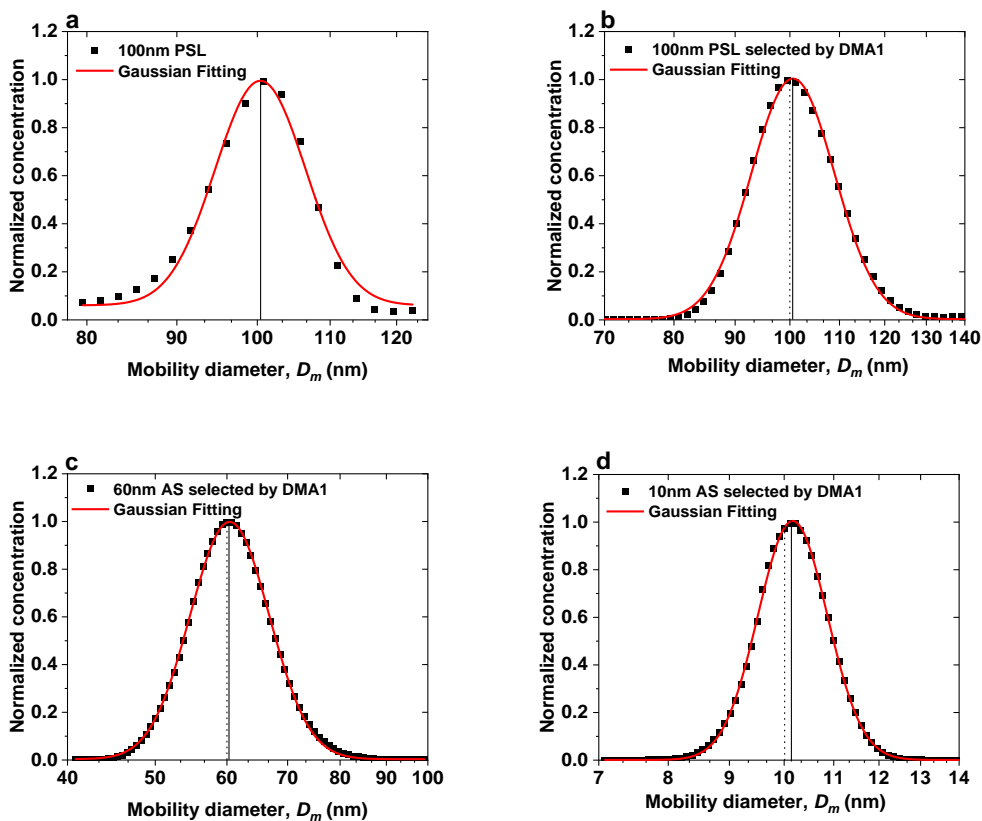
879

880

881

882

883

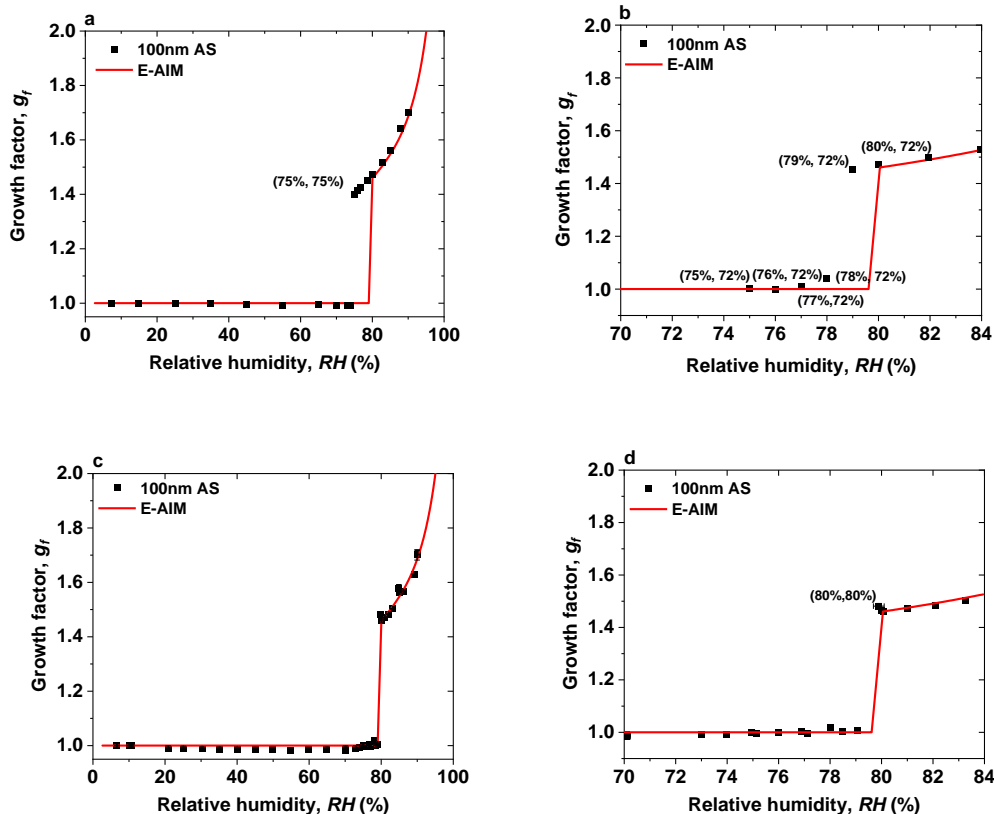


884

885

886 **Figure 3.** Sizing accuracy and sizing offset of nano-DMAs after calibration. (a) Normalized number size distribution
887 scanned by the nano-DMA2 for 100-nm PSL nanoparticles (black solid square). The black solid line marks peak
888 diameter from the Gaussian fits for the scan (red curve). Normalized number size distributions scanned by the nano-
889 DMA2 for 100-nm PSL nanoparticles (b), 60-nm (c), and 10-nm (d) ammonium sulfate (AS) selected by the nano-
890 DMA1 at RH below 5% at 298 K (black solid square). The dotted lines mark the diameters of the monodispersed
891 nanoparticles selected by the nano-DMA1, i.e., 100 nm in (b), 60 nm in (c) and 10 nm in (d). The black solid lines
892 mark the peak diameters from the Gaussian fits (red curve).

893



894

895

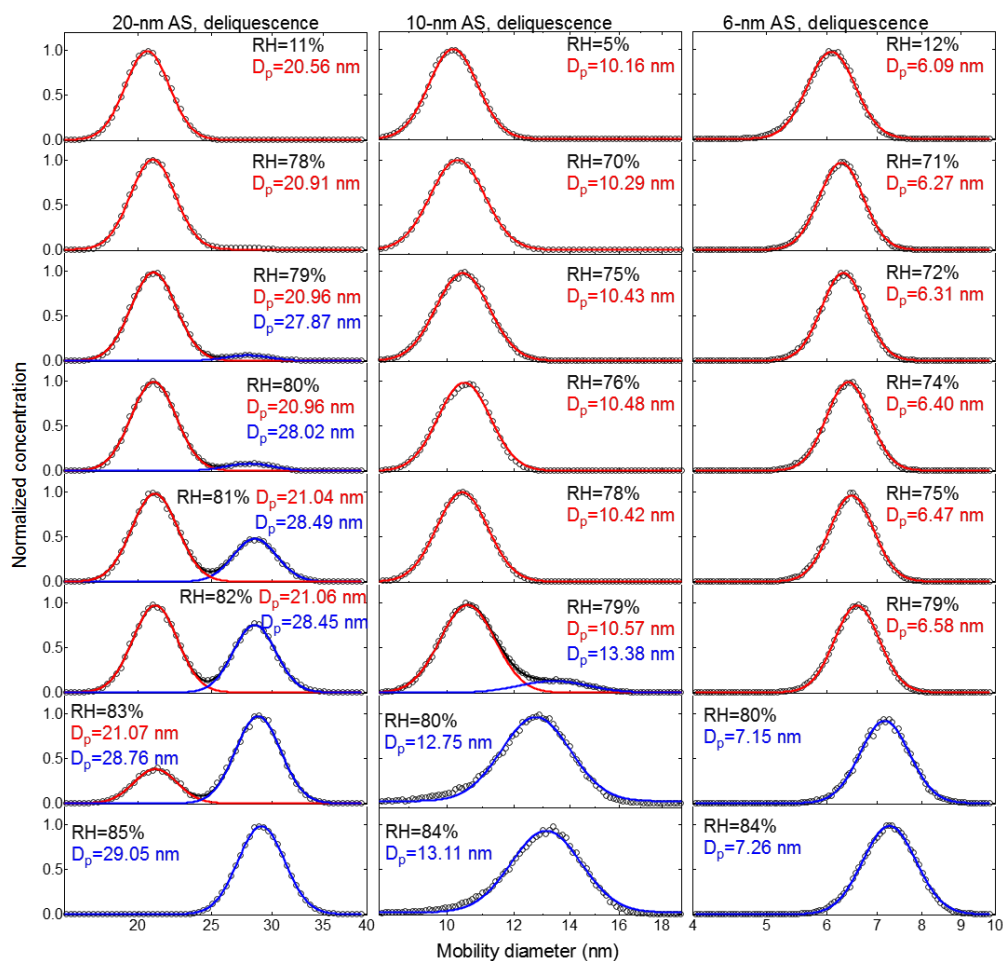
896 **Figure 4.** Mobility-diameter hygroscopic growth factors (g_f) of 100-nm ammonium sulfate (AS) nanoparticles at 298
 897 K measured in deliquescence mode. In comparison, the E-AIM model predicted growth factors of ammonium sulfate
 898 nanoparticles at 100 nm. (a) $RH_e = RH_a$, (75%, 75%) represents the (RH_e , RH_a), (b) $RH_e \geq RH_a + 3\%$, (75%, 72%)
 899 represents the (RH_e , RH_a), and (c) $RH_s = RH_a$. (d) The enlarged view of the RH range of 70% to 84% in Fig. 4c, (80%,
 900 80%) represents the (RH_s , RH_a). RH_s and RH_e are the RH of sheath flow in the inlet of nano-DMA2 and in the excess
 901 air line, respectively; RH_a is the RH of aerosol flow in the inlet of nano-DMA2.

902

903

904

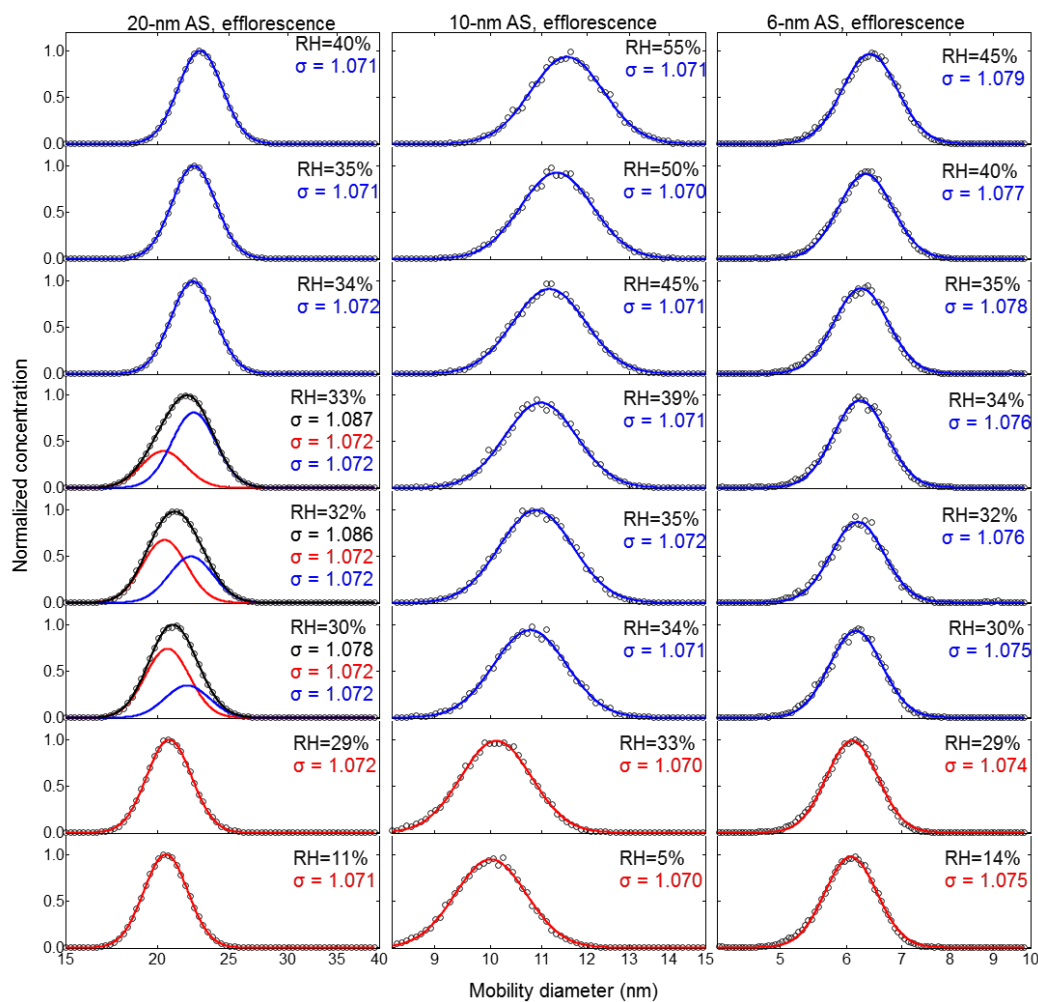
905



906

907 **Figure 5.** Deliquescence-mode measurements of ammonium sulfate (AS) aerosol nanoparticles with dry mobility
 908 diameter from 20-6nm. The measured (black square) and fitted (solid lines) normalized size distribution are shown for
 909 increasing RH. The RH history in each measurement is 5% → X%, where X is the RH value given in each panel.

910



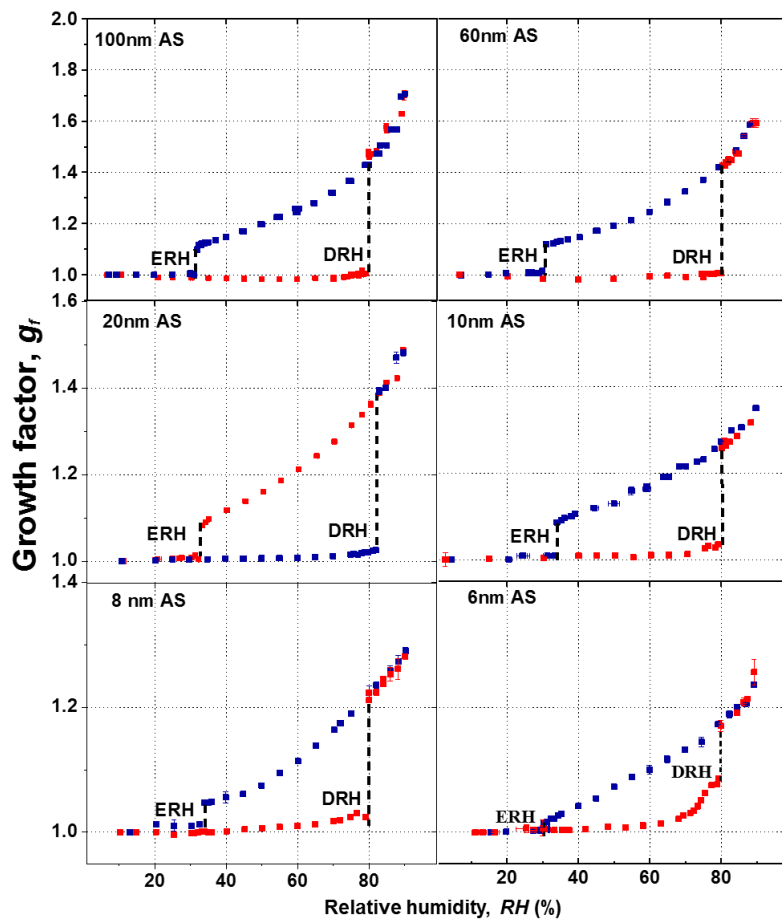
911

912 **Figure 6.** Efflorescence-mode measurements of ammonium sulfate (AS) aerosol nanoparticles with dry mobility
913 diameter from 20-6nm. The measured (black circle) and fitted (solid lines) normalized size distribution are shown for
914 increasing RH. The RH history in each measurement is 5%→97%→X%, where X is the RH value given in each panel.

915

916

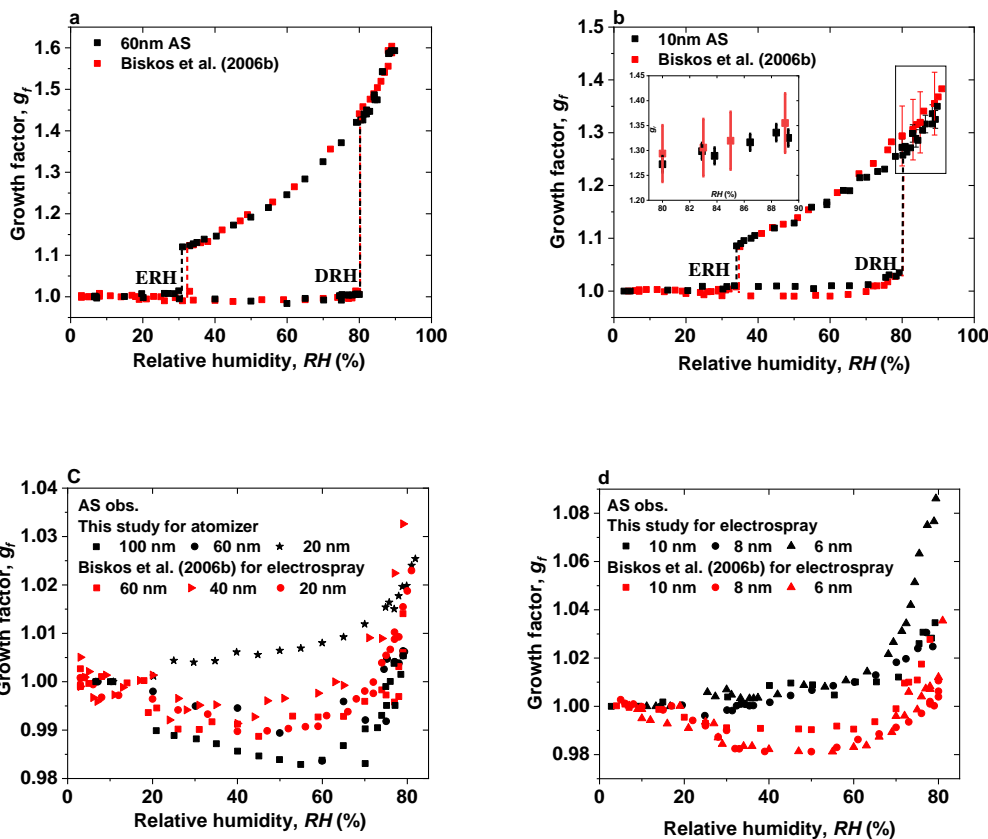
917



918

919 **Figure 7.** Mobility-diameter hygroscopic growth factors (g_r) of ammonium sulfate (AS) aerosol nanoparticles with dry
920 mobility diameter from 6 to 100 nm in the deliquescence mode (red square and error bar) and the efflorescence mode
921 (royal square and error bar). Deliquescence, and efflorescence relative humidity (DRH&ERH, black dashed line) of
922 ammonium sulfate (AS) nanoparticles with dry mobility diameter from 6 to 100 nm.

923



924

925

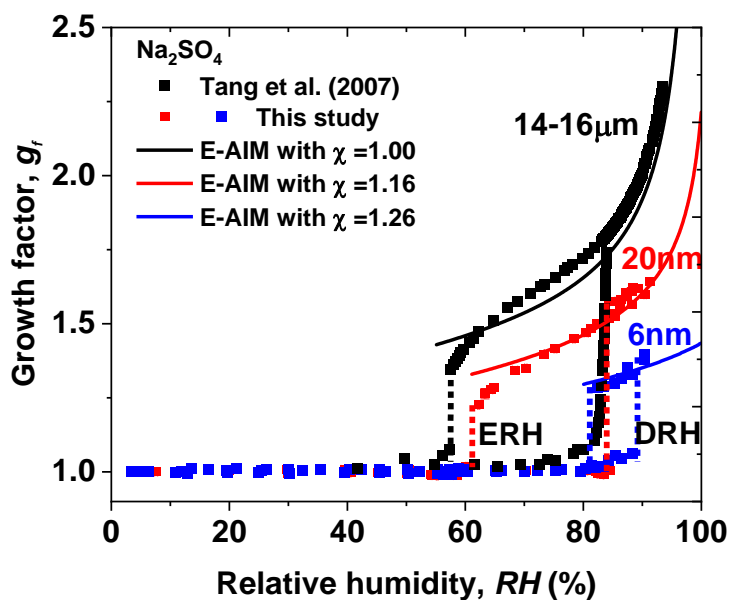
926 **Figure 8.** (a-b) Mobility-diameter hygroscopic growth factors (g_f , black squares), deliquescence and efflorescence
 927 relative humidity (DRH&ERH, black dashed lines) of ammonium sulfate (AS) nanoparticles with dry diameter 60 and
 928 10 nm, respectively. Red squares and dashed lines show the respective results from Biskos et al. (2006b), respectively.

929 Black and red uncertainties of growth factors at certain RH are calculated by $\sqrt{\left(\left(g_f \frac{\sqrt{2}\epsilon_{Dp}}{D_p}\right)^2 + \left(\epsilon_{RH} \frac{dg_f}{dRH}\right)^2\right)}$, where

930 ϵ_{Dp} , ϵ_{RH} , and g_f are uncertainty of particle mobility diameter, uncertainty of relative humidity, and growth factor with
 931 respect to RH, respectively (Mochida and Kawamura 2004). (c-d) Comparison of growth factors of ammonium sulfate
 932 (AS) nanoparticles with dry diameter range from 6 to 100 nm with Biskos et al. (2006b) prior to deliquescence of
 933 ammonium sulfate nanoparticles.

934

935



936

937 **Figure 9.** Mobility-diameter hygroscopic growth factors (g_r), deliquescence and efflorescence relative humidity
938 (DRH&ERH, red and blue dashed lines) of sodium sulfate nanoparticles with dry diameter 20 (red square) and 6 (blue
939 square) nm, respectively. Black squares and dashed lines show the respective results from Tang et al. (2007) with
940 electrodynamic balance (EDB), respectively. In this study, the black, red, and blue curves show E-AIM predictions,
941 including the Kelvin effect and shape factors (χ).

942

943

944

945

946

947

948